Contrast-enhanced magnetic resonance angiography.

Svensson, Jonas

Published in:
Acta Radiologica

DOI:
10.1034/j.1600-0455.44.s.429.1.x

2003

ACTA RADIOLOGICA SUPPLEMENTUM
Volume 44, Suppl. 429, 2003, BLACKWELL MUNKSGAARD, COPENHAGEN

CONTRAST-ENHANCED MAGNETIC RESONANCE ANGIOGRAPHY

Development and optimization of techniques for paramagnetic and hyperpolarized contrast media

JONAS SVENSSON

LUND UNIVERSITY

Department of Radiation Physics, Institute of Radiology and Physiology, Malmö, Malmö University Hospital, Lund University, SE-205 02 Malmö, Sweden

ABSTRACT

Svensson J. Contrast-Enhanced Magnetic Resonance Angiography. Development and optimization of techniques for paramagnetic and hyperpolarized contrast media. Stockholm 2001. ISBN 91-628-5322-8.

Contrast-enhanced magnetic resonance angiography (CE-MRA) is a diagnostic method for imaging of vascular structures based on nuclear magnetic resonance. Vascular enhancement is achieved by injection of a contrast medium (CM). Studies were performed using two different types of CM: conventional paramagnetic CM, and a new type of CM based on hyperpolarized (HP) nuclei.

The effects of varying CM concentration with time during image acquisition were studied by means of computer simulations using two different models. It was shown that a rapid concentration variation during encoding of the central parts of *k*-space could result in signal loss and severe image artifacts. The results were confirmed qualitatively with phantom experiments.

A postprocessing method was developed to address problems with simultaneous enhancement of arteries and veins in CE-MRA of the lower extremities. The method was based on the difference in flow-induced phase in the two vessel types. Evaluation of the method was performed with flow phantom measurements and with CE-MRA in two volunteers using standard pulse sequences. The flow-induced phase in the vessels of interest was sufficient to distinguish arteries from veins in the superior-inferior direction. Using this method, the venous enhancement could be extinguished.

The possibility of using HP nuclei as CM for CE-MRA was evaluated. Signal expressions for a flow of HP CM imaged with a gradient echo sequence were derived. These signal expressions were confirmed in phantom experiments using HP ^{129}Xe dissolved in ethanol.

Studies were also performed with a new CM based on HP ^{13}C. The CM had very long relaxation times ($T_{1,\text{in vivo}}/T_{2,\text{in vivo}} \approx 38/1.3$ s). The long relaxation times were utilized in imaging with a fully balanced steady-state free precession pulse sequence (trueFISP), where the optimal flip angle was found to be 180°. CE-MRA with the ^{13}C-based CM in rats resulted in images with high vascular SNR ($\sim$500).

CE-MRA is a useful clinical tool for diagnosing vascular disease. With the development of new contrast media, based on hyperpolarized nuclei for example, there is a potential for further improvement in the signal levels that can be achieved, enabling a standard of imaging of vessels that is not possible today.

Key words: magnetic resonance, angiography; contrast-enhanced MRA; hyperpolarized.

Jonas Svensson
Department of Radiation Physics, Institute of Radiology and Physiology, Malmö, Malmö University Hospital, Lund University, SE-205 02 Malmö, Sweden

LIST OF PAPERS

This thesis is based on the following papers:

I. SVENSSON J., PETERSSON J. S., STÅHLBERG F., LARSSON E.-M., LEANDER P. & OLSSON L. E.: Image artifacts due to a time varying contrast medium concentration in 3-D contrast-enhanced MRA. J. Magn. Reson. Imaging 10 (1999): 919–928.

II. SVENSSON J., LEANDER P., MAKI J. H., STÅHLBERG F. & Olsson L. E.: Separation of arteries and veins using flow-induced phase effects in contrast-enhanced MRA of the lower extremities. Magn. Reson. Imaging 20 (2002): 49–57.

III. JOHANSSON E., SVENSSON J., MÅNSSON S., PETERSSON J. S., OLSSON L. E., GOLMAN K. & STÅHLBERG F.: Gradient echo imaging of flowing hyperpolarized nuclei: theory and measurements on xenon dissolved in ethanol. J. Magn. Reson. 159(1) (2002): 68–75.

IV. SVENSSON J., MÅNSSON S., JOHANSSON E., PETERSSON J. S. & OLSSON L. E.: Hyperpolarized ^{13}C MR angiography using trueFISP. Magn. Reson. Med. (2003), accepted for publication.

CONTENTS

LIST OF ABBREVIATIONS

1-D	One dimensional
2-D	Two dimensional
3-D	Three dimensional
CE	Contrast-enhanced
CE-MRA	Contrast-enhanced magnetic resonance angiography
CM	Contrast medium
CNR	Contrast-to-noise ratio
CPMG	Carr–Purcell–Meiboom–Gill
DNP	Dynamic nuclear polarization
FA	Flip angle
FISP	Fast imaging and steady precession
FLASH	Fast low angle shot
FOV	Field of view
HP	Hyperpolarized
MIP	Maximum intensity projection
MR	Magnetic resonance
MRA	Magnetic resonance angiography
MRI	Magnetic resonance imaging
r_1	Longitudinal relaxation rate
r_2	Transversal relaxation rate
RARE	Rapid acquisition with relaxation enhancement
RF	Radio frequency
SNR	Signal-to-noise ratio
SSFP	Steady state free precession
T_1	Longitudinal relaxation time
T_2	Transversal relaxation time
TE	Echo time
TOF	Time-of-flight
TR	Repetition time
TrueFISP	True fast imaging and steady precession
v	velocity
V_{enc}	Velocity encoding

CONTRAST-ENHANCED MAGNETIC RESONANCE ANGIOGRAPHY

Development and optimization of techniques for paramagnetic and hyperpolarized contrast media

JONAS SVENSSON

INTRODUCTION

Magnetic resonance imaging (MRI) is a diagnostic modality capable of producing cross-sectional images of the body with unsurpassed soft tissue contrast. Since it was clinically introduced (around 1980), mostly morphological information has been obtained, and it was soon discovered that it was possible to obtain angiographic images. Following the technical development, the interest in MR angiography (MRA) has increased over the years.

There are several methods for performing angiography with MRI. Early methods relied on the flow of blood (2, 24, 63, 67, 81). The most common of these flow-based techniques are the time-of-flight (TOF) (42, 55) and phase contrast techniques (23, 24, 46, 92). The practical use of these methods is, however, limited due to long acquisition times and the complexity of vascular orientation and blood flow.

During the first half of the 1990s MR angiography was developed further with the use of an intravenously administered T_1-reducing contrast medium (CM) (16, 19, 69, 76, 77). By timing the CM injection to arrive in the vessels of interest during image acquisition, it was possible to achieve exclusive arterial enhancement (99, 101, 102). The introduction of this contrast-enhanced (CE) technique was the start of the major clinical breakthrough of MRA for many parts of the body. In just a few years, it has emerged as clinical routine and today it is possible to generate 3-D angiographic datasets in the order of 10 s (39).

The standard Gd-based contrast media used in Contrast-enhanced magnetic resonance angiography (CE-MRA) today are extracellular and have a short vascular half-life. Consequently, it is important to time the injection and the image acquisition carefully to ensure imaging during the first passage of the CM bolus in the vessels of interest. Improper timing of the acquisition could lead to a degradation of image quality or even to severe image artifacts (paper I, 74).

Another category of MR contrast medium, albeit still under development, is the blood pool agents (57, 61, 108). These intravascular CM have long vascular half-lives and hence imaging may be performed during steady-state concentration of the contrast medium. This is an attractive approach since the long period with steady-state concentration can be utilized for longer imaging times, which can increase the signal-to-noise ratio (SNR) or the spatial resolution in the angiograms. A problem with imaging during steady-state concentration, however, is the contemporary enhancement in arteries and veins. Since the two vessel types often run close to each other, similar signals make it difficult to differentiate them in the angiogram.

To enable a standard of imaging of vascular structures that has not been possible before, there is an interest in increasing the SNR in CE-MRA further. One way of doing this could be through the use of a fundamentally new type of CM, based on so-called hyperpolarized (HP) nuclei. The techniques for hyperpolarization result in polarization levels that are $\sim 10^5$ times higher than thermal equilibrium polarization at clinical field strengths. In 1994, it was demonstrated that it is possible to acquire *in vivo* MR images of HP ^{129}Xe (1). Following these initial experiments, both HP ^{3}He and ^{129}Xe has been used for *in vivo* imaging which has mainly been of the respiratory system (72, 86, 109, 110), but the use of these gases for angiographic imaging has also been suggested (11, 18, 87). Furthermore, it has recently been demonstrated that it is possible to hyperpolarize ^{13}C in certain molecules and to acquire MR angiograms after intravenous injection of the substance (36, 37, 120).

Imaging of a hyperpolarized substance differs from traditional MR imaging of thermally polarized ^{1}H, since there is no regrowth of longitudinal magnetization between the radio frequency (RF) pulses. Instead, the polarization decays continuously towards thermal equilibrium. Accordingly, there is

a need to evaluate the behavior of the signal from an HP substance during imaging, in order to optimize the pulse sequences and acquisition parameters used for CE-MRA.

Aim

The general aim of this thesis was to study and develop techniques for CE-MRA with conventional paramagnetic and new hyperpolarized CM, and to evaluate the usefulness of a new hyperpolarized CM based on ^{13}C. More specifically, the aims were:

- To study the image effects of a varying contrast medium concentration in the vessels during a 3-D CE-MRA acquisition. Also, to investigate the source of possible image quality degradation and artifacts and how to avoid them.
- To develop a postprocessing method for separation of arteries and veins in 3-D CE-MRA, and evaluate it in phantom experiments and in volunteer experiments.
- To perform theoretical and experimental studies of the signal behavior from a flowing hyperpolarized substance imaged with a spoiled gradient echo sequence.
- To evaluate a new CM based on HP ^{13}C for CE-MRA, and to acquire angiograms of living rats. Also, to study the signal behavior of a trueFISP pulse sequence in imaging of HP nuclei.

BACKGROUND

MR angiography without contrast enhancement

Before the introduction of contrast-enhanced MRA, the two most widely used methods for achieving vascular enhancement in MRI were based on blood flow. These methods, which are described briefly below, are called time-of-flight and phase contrast, and are still used for some applications.

Time-of-flight

In MR pulse sequences with short repetition time (TR), the magnetization is not allowed to fully recover longitudinally between RF pulses. Accordingly, the acquired MR signal decreases as the number of applied RF pulses increases, and becomes saturated (Fig. 1a). Blood flowing into an image slice has not experienced any RF pulses, and therefore gives a higher signal than the saturated surrounding stationary tissue (Fig. 1b) (33, 44). This effect is called inflow or time-of-flight (TOF). As the flowing spins travel further into the image slice, they experience more pulses and gradually become more saturated.

In TOF angiography (Fig. 2), a 2-D or 3-D spoiled gradient echo pulse sequence is used. The image plane is oriented perpendicular to the main flow direction to ensure fresh inflow of blood during imaging. In 2-D TOF (42, 55) multiple thin slices are acquired, increasing the probability of the blood experiencing only few RF pulses and giving a high signal. Accordingly, a large flip angle can be used, leading to efficient saturation of stationary tissue, and a high blood-tissue contrast. In 3-D TOF (76, 80, 106), the thicker imaging slab used makes the achievement of good blood-tissue contrast somewhat more troublesome. The use of lower flip angles is required in order to avoid blood signal saturation.

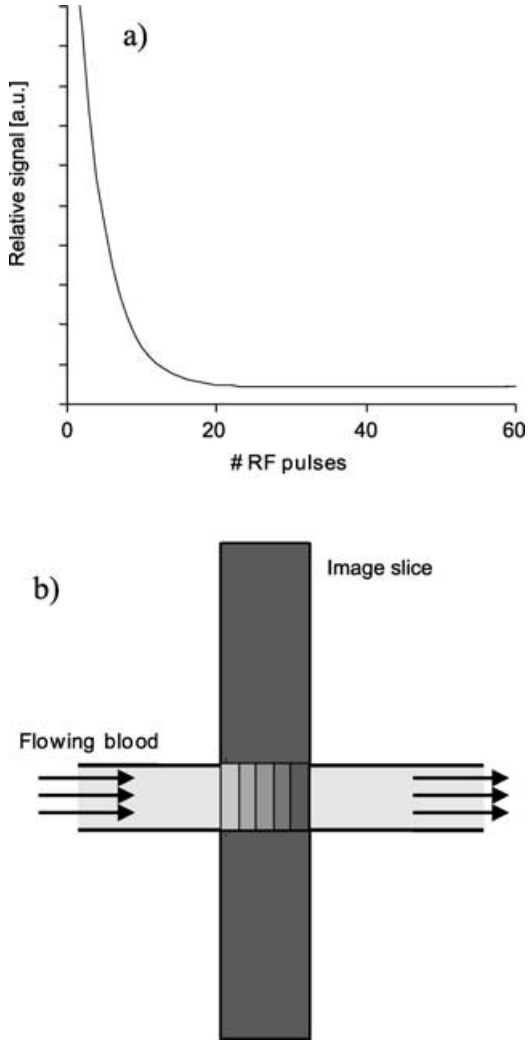

Fig. 1. (a) Blood signal saturation increases with increasing number of RF pulses and reaches a steady-state (TR = 10 ms, FA = 40°). (b) Blood flowing into an image slice experiences fewer pulses than the surrounding stationary tissue and therefore appears enhanced in the image.

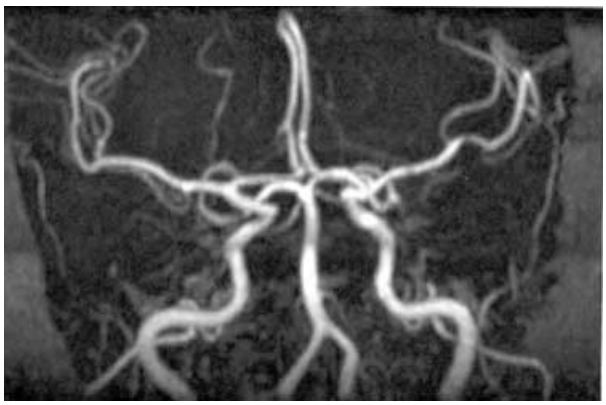

Fig. 2. Coronal maximum intensity projection (MIP) image from a 3-D TOF acquisition, covering normal intracranial vessels.

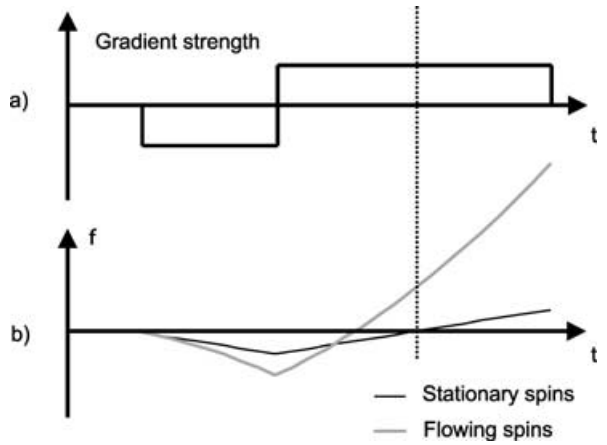

Fig. 3. During a bipolar gradient waveform (a), the phase accumulation (b) for stationary and flowing spins differs. While the stationary spins are rephased at the end of the bipolar gradient, flowing spins accumulate a phase proportional to the flow velocity.

However, through the use of excitation pulses with a varying flip angle over the slab, the saturation problems can be reduced. A flip angle increasing from a low value at the inflow side of the slab to a larger value at the other side of the slab results in a more uniform blood signal than a simple flat excitation pulse (62, 89, 98, 104). Another way of avoiding blood signal saturation is to acquire multiple thin image slabs rather than one thick slab (76, 91). This combines the benefits of thin slice imaging with the inherent advantages of 3-D imaging, e.g., high SNR and small voxel sizes. A presaturation pulse (28) can be used on the arterial outflow side of the 2-D slice pack or 3-D slab, to minimize enhancement from inflow of venous blood (55).

TOF angiography is limited by the requirements of choice of image plane and image volume thickness. However, it is still used, e.g., for visualization of arterial flow in the cranial region.

Phase contrast

While TOF angiography is based on manipulation of the magnitude of the magnetization, phase contrast angiography uses the accumulation of phase for flowing spins (23, 24). Under the influence of a linear magnetic field gradient, all spins accumulate a phase angle ϕ (Eq. 1), where γ is the gyromagnetic ratio, $G(\tau)$ is the gradient strength and $x(\tau)$ is the position of the spin (85).

$$\phi(t) = \int_{t_0}^{t} \omega \, \mathrm{d}\tau = \gamma \int_{t_0}^{t} G(\tau) x(\tau) \, \mathrm{d}\tau \qquad (1)$$

For stationary spins, $x(\tau)$ is a constant, and the totally accumulated phase at the end of a bipolar gradient waveform is zero. However, spins moving at constant velocity in the direction of the gradient accumulate a phase ϕ, proportional to the velocity, over the same time (Fig. 3). This difference for stationary and moving spins can be used to create an angiogram by displaying either the phase difference or the complex difference from two separate acquisitions obtained with opposite polarity of the bipolar waveform. Accordingly, flowing blood appears bright in this angiogram, and the signal in the phase difference image is directly proportional to the flow velocity.

By acquisition of four scans with different bipolar gradient waveform combinations in all three orthogonal directions, it is possible to generate phase contrast angiograms that are sensitive to flow in all directions (46, 92).

The flow sensitivity of a phase contrast pulse sequence is called the velocity encoding (V_{enc}), and is defined as the flow velocity resulting in a phase accumulation of 180°. Higher velocities result in larger phase angles, leading to phase aliasing that may be misinterpreted in the angiogram. In order to properly enhance vessels with certain flow velocities, the V_{enc} is adjusted by altering the amplitude and/or the duration of the velocity encoding gradients.

The sensitivity to flow velocity and the risk of aliasing makes the vascular enhancement in phase contrast angiograms complicated. Nevertheless, in evaluations of slow flow where the TOF method suffers from blood signal saturation, phase contrast angiography can be used successfully (10).

Contrast-enhanced MR angiography

The flow-based MRA methods (in section MR angiography without contrast enhancement) may

Fig. 4. Standard coronal CE-MRA of the pulmonary and thoracic vessels in a patient, obtained using a paramagnetic CM. Both arteries and veins are shown. The patient has dilated venous system from the left arm and cranially from the left subclavian vein a 3-cm in diameter vascular malformation is shown.

work well in certain regions of the body, e.g., in conditions of steady flow in mainly one direction. However, in cases with complex blood flow patterns, these methods are difficult to use. Furthermore, they are not practicable in regions of the body where a short acquisition time is a necessity. Contrast-enhanced magnetic resonance angiography (CE-MRA) (99, 102) is rather insensitive to disturbances due to complex flow patterns since it is not based on flow effects. The basis of CE-MRA is signal enhancement created by a CM injected into the vascular system. This enables imaging of large volumes with short acquisition times, without restrictions on flow direction (60, 73).

In clinical CE-MRA, vascular enhancement is currently obtained through the use of paramagnetic CM (Fig. 4). However, the recent success in hyperpolarizing certain nuclei has also created an interest in using CM based on HP substances to increase the SNR and contrast-to-noise ratio (CNR) of CE-MRA that can be achieved at present even further.

CE-MRA with paramagnetic contrast media

Several contrast media for MRI are available, and most of them are based on gadolinium (Gd) (68, 133). Gd is paramagnetic and reduces the relaxation times of the tissue in which it is present. How much the tissue relaxation times are reduced after administration of the CM depends on the CM relaxivities (r_1 and r_2), and on the concentration C (Eq. 2 (47)). For most of the CM on the market the relaxivities are approximately $r_1 \approx 4/\text{mM s}$ and $r_2 \approx 6/\text{mM s}$ at 1.5 T (7, 60). The reduced T_1 in tissues with CM uptake make them appear enhanced on T_1-weighted images.

$$\frac{1}{T_{1,\,\text{after}}} = \frac{1}{T_{1,\,\text{before}}} + r_1 \cdot C \tag{2a}$$

$$\frac{1}{T_{2,\,\text{after}}} = \frac{1}{T_{2,\,\text{before}}} + r_2 \cdot C \tag{2b}$$

Even though the Gd-based CM are extracellular and have relatively short vascular half-lives (~4 min) (68), they can be used for CE-MRA. The CM is administered intravenously, and the acquisition is timed to coincide with the first passage of the bolus in the vessels of interest (see below).

In CE-MRA, spoiled 3-D gradient echo pulse sequences with short TR are used for image acquisition. The transverse magnetization is assumed to be completely spoiled prior to each new RF pulse, and with a short TR, the signal S decreases with increasing number of excitations to a steady-state described by equation 3 (124).

$$S \propto \frac{(1 - \mathrm{e}^{-TR/T_1})}{1 - \cos(\alpha)\mathrm{e}^{-TR/T_1}} \sin(\alpha)\mathrm{e}^{-TE/T_2^*} \tag{3}$$

A high vascular signal is obtained due to the short T_1 of blood, which is a consequence of the CM administration. When $T_{1,\text{blood}} \ll T_{1,\text{tissue}}$ is fulfilled, the signal saturation in non-vascular tissue is more pronounced than for blood, and a high blood-tissue contrast is achieved (Fig. 5). A further advantage with the use of a short TR is that the acquisition times become very short, enabling, e.g., acquisition of complete 3-D data sets within a single breath-hold (39).

The timing of the image acquisition to the first passage of the bolus is important for optimal vessel enhancement and avoidance of CM leakage to the extra-vascular space during imaging. The acquired MR signal is stored in a raw data matrix (*k*-space), where the central parts correspond to low spatial frequencies, and the outer parts correspond to high spatial frequencies. Accordingly, image structure and contrast is encoded in the *k*-space center. It is therefore important that maximum CM

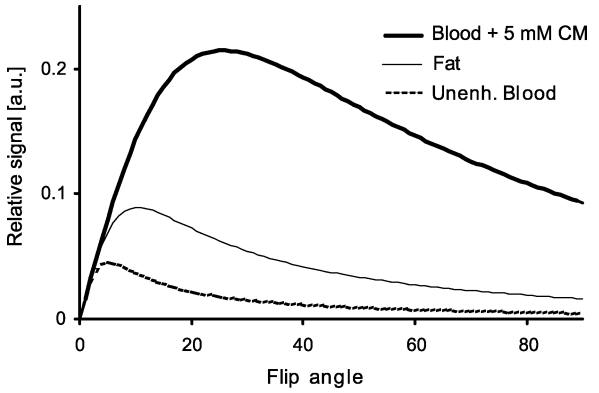

Fig. 5. The signal from blood without contrast enhancement is lower than the signal from fatty tissue. Assuming a 5-mM concentration of a Gd-based CM in the blood, the signal increases dramatically. A flip angle of approximately 25° maximizes the enhanced blood signal. The contrast between blood and fat, however, increases all the way up to 90°.

concentration is timed to coincide with sampling of this part of *k*-space to ensure maximal vascular enhancement. Furthermore, if CM concentration varies during image acquisition the acquired signal will vary correspondingly and acts as a filter applied to the *k*-space data (29, 43, 70). The ''filtered'' data may be misinterpreted by the Fourier transform during reconstruction of the CE-MRA image and result in image artifacts (15, 53, 74). To minimize the risk of artifacts, the injection should be timed so that concentration variations are small during encoding of the basic image contrast and structure (i.e., the center of *k*-space).

The point in time when the central *k*-space lines are encoded depends on the type of phase encoding scheme used in the pulse sequence. For standard 3-D imaging with linear phase encoding, two acquisition loops are used, corresponding to the two phase encoding directions. With this technique the central lines are encoded at half the acquisition time (101, 117). In a centric encoding scheme the most central *k*-space lines are instead encoded first in both phase encoding directions, filling the outermost parts of *k*-space at the end of the acquisition (113). A more elaborate technique, referred to as ''elliptical centric view order'', is to calculate the distance to the *k*-space center for each encoding line, and acquire them in order of increasing distance, leading to a more ''true'' centric encoding (135).

Regardless of the encoding scheme used, the timing of the bolus arrival is important. Several methods exist for achieving an accurate timing. A small test bolus can be injected, followed by acquisition each second of single 2-D images covering the vessels of interest. By measurement of the vascular signal in these images, the time from injection to arrival of the bolus can be calculated, and an appropriate delay between bolus injection and start of the CE-MRA acquisition can be chosen (25, 41, 117). It is also possible to let a pulse sequence monitor the signal from the vessels of interest after bolus injection, and automatically switch to the CE-MRA sequence upon bolus arrival (31, 100). With ''fluoroscopic'' MR imaging, the bolus arrival can be monitored visually, followed by manual switching to the CE-MRA pulse sequence (136). These latter two methods are preferably used together with a centric encoding scheme, ensuring that the central lines are acquired during peak CM concentration.

Instead of timing the image acquisition to the arrival of the bolus, the total imaging time can be shortened to allow for several acquisitions during passage of the bolus, resulting in visualization of the blood flow dynamics. This is referred to as time-resolved MRA, and makes bolus timing unnecessary. Instead, the most suitable of the acquired CE-MRA volumes (e.g., the one with peak arterial enhancement) can be chosen afterwards. Different methods can be used to achieve a sufficiently short imaging time. In the 3-D TRICKS method (14, 58), *k*-space is divided into several different parts, each part being sampled at different points in time. The low spatial frequencies are sampled more often than the less important high spatial frequencies. Each time-frame is then reconstructed by interpolation of the required parts of *k*-space sampled closest in time. This technique has been developed further through the use of undersampled projection reconstruction (94), to allow for even higher temporal and/or spatial resolution (125). Another approach for achieving short imaging times is to use partial sampling of the full *k*-space together with zero-filling (111). In parallel imaging (103, 114), several receiver coils are used simultaneously to increase the sampling efficiency. This has also been applied to time-resolved CE-MRA (36, 132). In some applications a 2-D MR digital subtraction approach is sufficient, enabling very short imaging times (49, 56, 130). Time-resolved MRA is well suited for imaging of vessels with a short arterial phase of peak CM concentration, such as the carotids, or the intracranial arteries (13), where long imaging times lead to venous overlay and difficulties in interpreting the angiograms. The possibility of following the CM dynamics in time-resolved MRA can also be used for artery-vein separation (see below).

Another type of contrast medium, the so-called blood pool agents, with long vascular half-lives are

under development (57, 61, 108). The contrast enhancement in these CM also relies on the T_1-reducing effect. Due to larger particle sizes, the relaxivities for these CM are higher than for conventional extracellular CM. The higher relaxivities result in shorter blood relaxation times if the same dose as for conventional CM is administered. Alternatively, similar blood relaxation times as for conventional CM may be reached with a lower dose. The long vascular half-lives eliminate the need for complicated timing procedures and instead permit longer acquisition times during the equilibrium phase of CM concentration. This can be used to increase the overall image quality through increased spatial resolution and/or number of signal averages (3, 40, 64). However, during CM equilibrium concentration, the enhancement is similar in both arteries and veins, leading to difficulties in interpreting the angiogram (3, 27, 40). The same effect may arise for extracellular CM if the timing is poor (45, 52, 118). Several methods have been proposed for separation of the two vessel types. Two different approaches based on the difference in accumulated phase between the two vessel types have been presented. One of them utilizes the difference in blood oxygenation and susceptibility (131), and the other makes use of the differences in blood flow (paper II, 8, 30). Other methods are based on the difference in the temporal enhancement patterns of arteries and veins following a CM bolus injection (9, 21, 54, 82, 83, 111). If the spatial resolution is sufficiently high, segmentation can be performed with pure image postprocessing techniques (66, 116, 122).

CE-MRA with hyperpolarized contrast media

Conventional proton MRI at thermal equilibrium polarization levels is an inherently insensitive technique. This is a consequence of the fraction of spins used for imaging being in the order of only 10^{-6} of the total number of spins available. However, in 1994 it was demonstrated that it is possible to acquire *in vivo* MR images of nuclei at non-thermal polarization (hyperpolarized) levels (1). By hyperpolarizing nuclei to a level of $\sim$10%, the sensitivity of MRI is increased by several orders of magnitude, and both hyperpolarized ^{129}Xe and ^{3}He have been used to obtain *in vivo* MR images of primarily the lungs and the airways (72, 86, 109, 110). Following the success of lung imaging, the use of the HP gases as a CM for CE-MRA has been proposed (11, 18, 78, 87). It has also been demonstrated that it is possible to hyperpolarize ^{13}C in certain molecules and use them for CE-MRA (paper IV, 38, 120).

The different nuclei are hyperpolarized using different methods. One of the most common methods for hyperpolarizing ^{3}He and ^{129}Xe is spin-exchange optical pumping (129). With this method the valence electron of an alkali metal (in general rubidium) is optically pumped with circularly polarized light, followed by transfer of polarization from the electron to the noble gas nucleus by spin exchange. ^{3}He can also be polarized through metastability-exchange optical pumping (4, 5, 35), and there is also a so-called ''brute-force'' technique under development (88). Hyperpolarization of ^{13}C for use in MRI has been demonstrated with two different methods, parahydrogen induced polarization (38) and dynamic nuclear polarization (DNP) (paper IV, 37, 120) (Fig. 6).

After polarization, the hyperpolarized nuclei must be administered to the vascular system. Helium has very low solubility in blood, thus excluding inhalation as a possible way of administration. However, the gas can be encapsulated in microbubbles in a suspension, and delivered by intravascular injection (12, 17, 18). Xenon is directly soluble in blood, and accordingly, inhalation is one possible way of vascular administration (86, 121, 128). Another way of administering xenon is to dissolve it in a biocompatible carrier (6, 22, 87, 137) to be injected into the vascular system. Hyperpolarized ^{13}C differs from ^{3}He and ^{129}Xe since it is part of a water-soluble molecule, and not a gas. Accordingly, it can be administered directly through intravascular injection with a much higher concentration than the gases.

The prerequisites for CE-MRA with a hyperpolarized CM are in many respects different from CE-MRA with a paramagnetic CM. The polarization of the nuclei decreases continuously with a time-constant T_1, and eventually reaches thermal equilibrium. Consequently, the T_1 has to be long enough to allow for transportation from the polarizer, for preparation of the CM prior to injection, for *in vivo* distribution to the vessels of interest, and for imaging. Furthermore, MR imaging of nuclei at non-thermal polarization levels requires a different pulse sequence methodology than for imaging with thermally polarized nuclei. The non-renewable magnetization is most often utilized either through multiple small flip angle excitations or with single-shot techniques. The gaseous HP nuclei have relatively short T_2* values *in vivo*, which has favored the use of the small flip angle techniques. Several different approaches are possible, e.g., the use of a standard FLASH-type pulse sequence with linear phase encoding (17). To minimize the echo time (TE), radial scanning with projection reconstruction can be useful (11). Interleaved

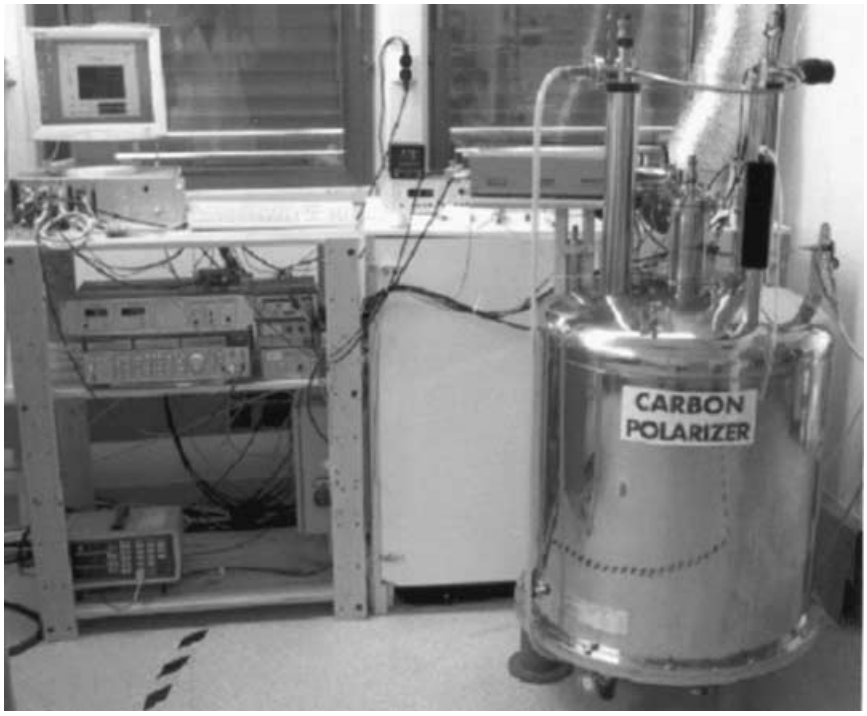

Fig. 6. Experimental set-up for polarizing ^{13}C using the DNP method.

spiral trajectories can be used to obtain a short total imaging time, e.g., for imaging of a dynamic distribution of a CM. For HP nuclei with long T_2 relaxation time (e.g., ^{13}C in the molecule used in paper IV), the available magnetization is better used if the transverse magnetization is recycled from one repetition to the next. This can be done with a steady-state free precession (SSFP) technique such as the true fast imaging and steady precession (trueFISP) pulse sequence (90). This sequence is also called balanced fast field echo. With fully balanced gradients and an alternating $\pm\ \theta$ flip angle, the magnetization reaches a coherent steady-state in imaging at thermal levels. However, for HP imaging, no steady-state is reached (paper IV). If the relaxation times of the CM are long enough, large flip angles can be used during this ''pseudo'' steady-state, and it is possible to use almost the full magnetization. In this case the trueFISP sequence actually becomes similar to the single-shot rapid acquisition with relaxation enhancement (RARE) pulse sequence (48). To make optimal use of the different pulse sequences used for imaging of HP substances, new signal expressions have been developed (paper III, paper IV, 34).

Another interesting aspect of *in vivo* imaging of nuclei other than ^{1}H is that the signal is acquired directly from the HP nuclei, and tissues in which the HP nuclei are not present will have zero signal. This leads to a dramatic increase in the CNR for the enhanced tissue.

The transient nature of the polarization of the HP CM makes longer transportation of it difficult. The HP gases can be stored in glass cells in an external static magnetic field with T_1 in the order of hours, prior to CM preparation. For HP ^{13}C, the T_1 is about 80 s in water solution (paper IV). Consequently, the CM is preferably hyperpolarized on-site to ensure a high polarization level at the time of use. Nevertheless, ^{3}He-enhanced images have been produced after long distance airborne transport of the HP gas (134).

Apart from the differences already mentioned, there are also similarities between paramagnetic CM and HP CM. For example, the bolus timing issues discussed in section CE-MRA with paramagnetic contrast media and in paper I are general and do also apply to HP CM. For an intravascular HP CM, the artery-vein separation (paper II and section CE-MRA with paramagnetic contrast media) also becomes important.

MATERIALS AND METHODS

This thesis is based on work with two different types of contrast media: paramagnetic and hyperpolarized.

The methodologies for the use of these two types of CM are rather different, and consequently this Material and Methods section is divided into two parts.

In section Paramagnetic contrast media, paramagnetic CM is used for studies of the effects of a time-varying CM concentration during imaging (paper I), and for development of a postprocessing method capable of separating arteries from veins (paper II).

In section Hyperpolarized contrast media, the possibility of using hyperpolarized nuclei as CM for CE-MRA is evaluated. The behavior of signal from flowing HP nuclei during imaging with a spoiled gradient echo pulse sequence is studied theoretically and with flow phantoms (paper III). A new CM based on HP ^{13}C is used for CE-MRA in living rats, using an optimized trueFISP pulse sequence (paper IV).

Paramagnetic contrast media

MR systems and pulse sequences

A Magnetom Vision 1.5 T MR system (Siemens AG, Erlangen, Germany) and the head coil (paper I) or the extremity coil (paper II) was used for all measurements except the volunteer experiment with the blood pool agent (paper II), where an NT 1.5 T system (Philips Medical Systems, Best, the Netherlands) equipped with an extremity coil was used.

All angiographic experiments were performed with standard 3-D spoiled gradient echo sequences, used clinically for CE-MRA. Acquisition times were less than 1 min. All images were obtained in coronal view with the image phase encoding in the right-left direction (superior-inferior readout direction).

Simulation of a time-varying contrast-medium concentration

Image artifacts may arise in CE-MRA if the CM concentration varies during imaging. These effects were studied with two different simulation models, a 1-D model and a 3-D model (paper I).

Models

The 1-D model deals with the mathematical aspects of the Fourier transform used for image reconstruction and is not directly related to MR imaging. This model was used to perform basic simulations with ideal bolus shapes. It reduces the studies of effects from CM variation in 3-D CE-MRA to one dimension by assuming that the concentration variation during execution of the inner phase encoding loop (slice) and over a single TR is negligible. Hence, only the effects of a varying concentration during the outer phase encoding loop are assumed to be relevant.

A line profile from an idealized MR image covering a nonenhanced vessel (e.g., the aorta) and surrounding tissue (e.g., fat) is divided into two parts; one containing only the vascular signal and one containing only the signal from the surrounding tissue. The profile with vascular signal is Fourier transformed to get a line of raw data, $S_{\text{aorta}}(k_x(t))$. The time between acquisitions of two data points in these raw data corresponds to the time to complete one repetition of the outer phase encoding loop. To simulate the varying CM concentration during acquisition, $S_{\text{aorta}}(k_x(t))$ is multiplied (pixel by pixel) by a factor, $\text{SR}(t)$, corresponding to the signal enhancement from the CM at any given time. The inverse Fourier transform of this product yields the contrast-enhanced vascular signal profile, $M_{\text{aorta}}(x)$ (Eq. 4), which is recombined with the tissue part to give the total line profile.

$$M^{\text{CE}}_{\text{aorta}}(x) = FT^{1}\{SR(t) \cdot S_{\text{aorta}}(k_x(t))\} \qquad (4)$$

The 3-D model (97) is based on the *k*-space formalism (71, 123) in combination with a multidimensional partition concept. It can be used for more advanced simulations, taking into account several aspects of a 3-D CE-MRA experiment simultaneously, e.g., 3-D image formation, pulsatile flow (95), and CM concentration variation. It is capable of simulating MR images for any general steady-state free precession (SSFP) pulse sequence (96).

Simulations

In all simulations, it was assumed that a 3-D spoiled gradient echo sequence similar to a standard CE-MRA pulse sequence was used. An ideal 10 s CM bolus was simulated with the 1-D model for four different injection timings (Fig. 7). Furthermore, the importance of including surrounding tissue in the model was demonstrated by performing simulations both with and without surrounding fatty tissue.

To investigate whether or not the effects of a varying CM concentration appear similar in the two models, simulations with the 3-D model were performed using the same bolus timings as in the 1-D model (Fig. 7). Effects from flow were not included in these simulations. In the remaining simulations with the 3-D model, the goal was to imitate a real CE-MRA experiment; hence typical CM dynamics (32) and pulsatile blood flow for the

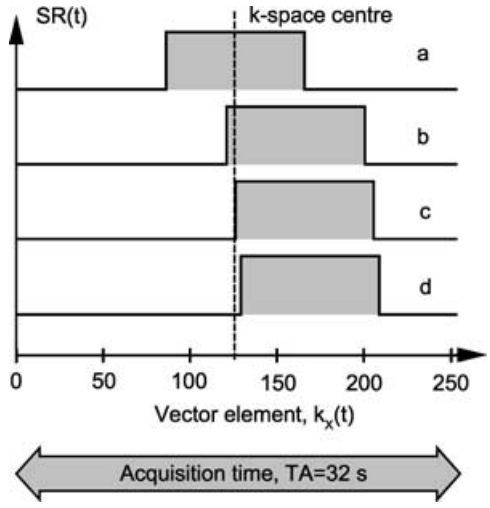

Fig. 7. Relative signal enhancement SR(*t*) for the four different bolus timings used in simulations with model I (and model II). An ideal 10-second long bolus shape is used; *k*-space center is sampled after half the acquisition time (linear phase-encoding). In (a) the bolus is centered in *k*-space. In (b), (c), and (d) the bolus arrives 4, 5 and 6 s later than in (a), respectively.

descending aorta were used. See Fig. 8 for an example of timings.

Separation of arteries and veins

Simultaneous enhancement of both arteries and veins in an angiogram may cause difficulties in separating them visually. To overcome such problems in the lower extremities a postprocessing method capable of extinguishing the veins in a CE-MRA image volume was developed (paper II).

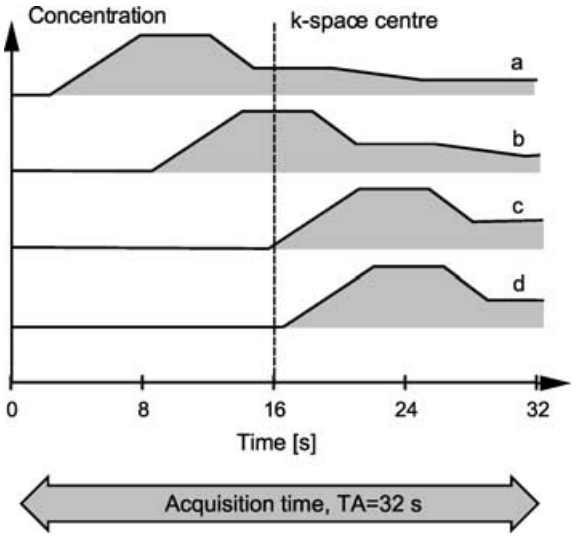

Fig. 8. Example of bolus timings for the CM, used in patient-like bolus dynamics simulations with the 3-D model. Peak CM concentration arrives 13 s early (a) compared with a centered bolus, (b) centered in *k*-space, (c) 13 s late, (d) 15 s late.

Basis

The blood flow in the arteries and the veins of the lower extremities is mainly directed superior-inferior. In the 3-D gradient echo pulse sequences used for CE-MRA, a bipolar readout gradient is commonly used in the same direction. The spins in blood flowing in the direction of a bipolar gradient accumulate a phase angle proportional to the flow velocity (Eq. 1). Accordingly, the opposite flow direction of arterial and venous blood results in a difference in flow-induced phase. This phase difference can be used for separation of the two vessel types (Fig. 9).

Segmentation process

Separation of the arteries and veins was performed in three steps (Fig. 10). Two different methods for performing the first step were evaluated: simple global thresholding, and a form of local thresholding (105). Global segmentation is based on a single threshold value over the entire 3-D phase image volume, whereas the local thresholding is based on an individual threshold for each pixel. This local threshold is calculated from a small region of neighboring pixel values. Global thresholding requires a phase-subtraction in order to remove all phase effects other than those caused by flow. Local thresholding is less sensitive to global phase variations and may be used even without subtraction.

The result of the above segmentation process is an image volume where all pixels are marked either as artery or vein. To find out which of the pixels are actually part of a vessel (step 2), the contrast-enhanced magnitude image volume was used. A global signal threshold value was chosen, and all pixels with signal values above the threshold were considered contrast-enhanced and thereby part of a vessel. This threshold was chosen manually.

In the third step, all pixels that were identified as being both vein and vessel in the two previous steps were adjusted to zero intensity in the CE-MRA magnitude image volume in order to extinguish the veins.

Flow phantom measurements

The effects of a varying CM concentration simulated in section Simulation of a time-varying contrast-medium concentration were studied qualitatively using a phantom imitating an aorta (paper I). Regular tap water doped to the T_1 of blood

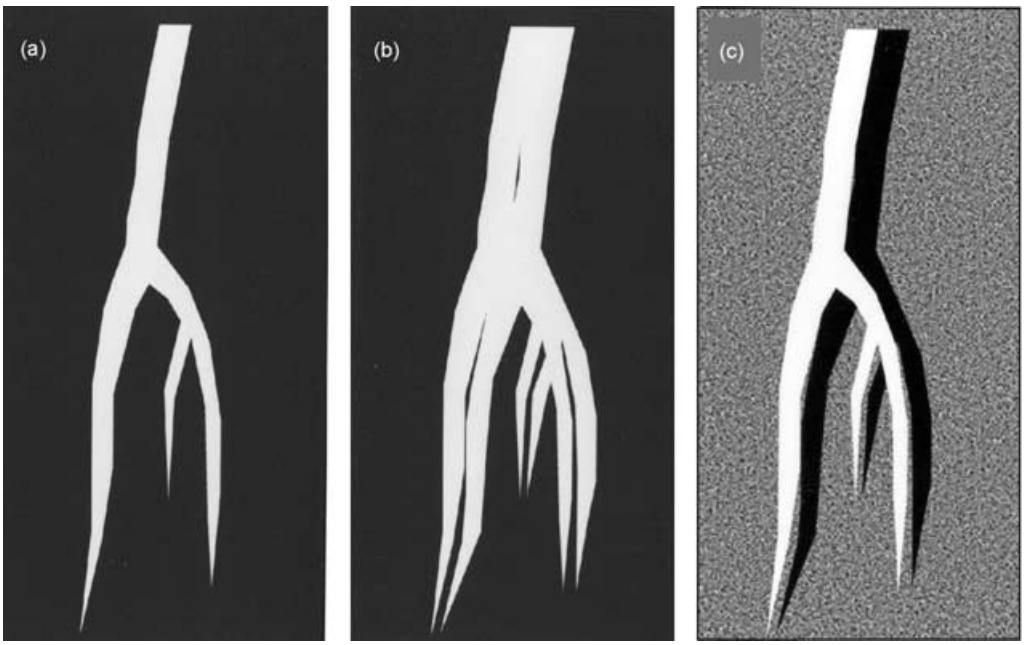

Fig. 9. Hypothetical magnitude images from CE-MRA experiment. Ideally images are acquired with exclusive arterial enhancement (a), but with the use of a blood pool agent or through poor timing of a CM, simultaneous arterial and venous enhancement may occur (b). The similar arterial and venous signal in (b) makes it difficult to differentiate between them. However, the arterial and venous signals in the corresponding phase image (c) differ due to opposite flow directions, and can be used for separation of the two vessel types.

($\sim$1200 ms) was used as flowing medium ($v = 105$ cm/s).

A standard CE-MRA pulse sequence was used together with two different timings of a bolus injection (45 mL, 50 mM Gd^{3+}):

- Good timing – the center of the bolus arriving during acquisition of the central *k*-space lines
- Poor timing – bolus arriving too early.

The postprocessing method for separation of arteries and veins (section Separation of arteries and veins) was evaluated with a flow phantom containing two equal-sized plastic pipes with opposite directed flow (paper II). Distilled water doped with Gd^{3+} was used to simulate contrast-enhanced blood flowing through the pipes. Imaging was performed at five different mean flow velocities: 0, 9, 15, 65 and 80 cm/s. Two image volumes were acquired with a 3-D CE-MRA pulse sequence for each flow velocity, one in flow-compensated mode and one without flow compensation. After subtraction of these two image volumes, the phase accumulation due to flow was measured for the different flow velocities. The measured values were compared with values calculated according to Eq. 1. Post-processing (section Separation of arteries and veins) in order to extinguish the flow in one direction was performed for the lower flow velocities (9 and 15 cm/s).

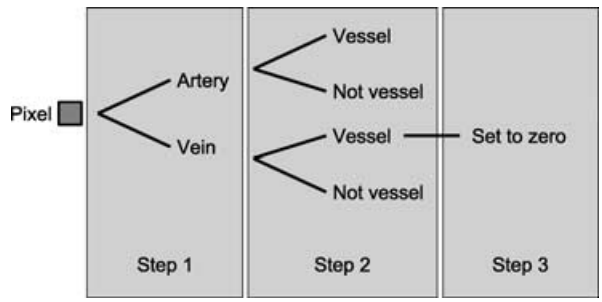

Fig. 10. Separation of arteries and veins. (1) All pixels in the image volume were marked either as artery or as vein. (2) All pixels in the image volume were marked either as vessel or not vessel. (3) Veins were extinguished by setting all pixels marked both as 'vein' and 'vessel' to zero.

Contrast media

The artery-vein separation method described in section Separation of arteries and veins was evaluated (section Volunteer measurements) for a poor injection timing of an extracellular CM (Omniscan, Nycomed, Oslo, Norway), and for steady-state concentration of a blood pool agent (MS-325, EPIX Medical, Cambridge, MA, USA). Omniscan is a conventional Gd-based (Gd-DTPA-BMA) extracellular CM. MS-325 is an investigational blood pool agent based on a Gd-chelate that binds strongly, but reversibly, to human serum albumin in plasma (64).

Volunteer measurements

CE-MRA was performed in the lower leg of two volunteers to evaluate the artery-vein separation method (paper II), one using a poor timing of the extracellular CM and one using equilibrium concentration of the blood pool agent (section Contrast media).

Before administration of the extracellular CM, one image volume was acquired to be used for background subtraction. Following a bolus injection of the CM, three CE-MRA image volumes where acquired. The first acquisition was timed to enhance the arteries only. The two later volumes were deliberately acquired with poor timing to obtain both arterial and venous enhancement, one flow-compensated, and one not flow-compensated. Artery-vein separation was performed using the latter two acquired volumes.

CE-MRA using the blood pool agent was performed approximately 45 min after injection of the CM. Two image volumes were acquired, one using flow compensation, and one without flow compensation. Four averages were used in both acquisitions. No precontrast images were acquired.

Hyperpolarized contrast media

MR systems and pulse sequences

All imaging experiments were performed using a 2.35 T animal MR scanner (Biospec 24/30, Bruker Biospin, Ettlingen, Germany) equipped with a double-tuned (^{1}H and ^{129}Xe/^{13}C) birdcage coil.

The signal from flowing HP ^{129}Xe was studied using a gradient spoiled 2-D gradient echo sequence with the parameters: TE/TR = 6/12 ms, FOV = $60 \times 45\,mm^2$, matrix = 64×32 (paper III).

Experiments with HP ^{13}C were performed using a trueFISP pulse sequence (TE/TR = 1.8/3.6 ms, FOV = $70 \times 70\,mm^2$, matrix = 64×64) (paper IV). To avoid excessive signal oscillation, a preparatory RF pulse always preceded the imaging sequence. The flip angle of this prepulse was half of what was used in the imaging sequence, forcing the magnetization into a pseudo steady-state (20). After each image acquisition the remaining magnetization was rewound and stored in the longitudinal direction using a corresponding "flip-back" RF pulse, enabling further imaging after an arbitrary time delay.

Hyperpolarization and preparation of ^{129}Xe and ^{13}C

^{129}Xe was polarized using a commercial polarizer (IGI. 9600 Xe, Amersham Health, Durham, NC) (paper III). The polarized gas was dissolved in ethanol (95%) immediately prior to the flow phantom experiments (section Flow phantom experiments using HP ^{129}Xe). Ethanol was a suitable carrier of the gas in the phantom experiments due to its high solvent characteristics for xenon (Ostwald coefficient = 2.5 at 20°C) (50), and the long T_1 relaxation time of the dissolved ^{129}Xe (~50 s).

A new CM based on ^{13}C incorporated in the water-soluble molecule bis-1,1-(hydroxymethyl)-1–^{13}C-cyclopropane-D_8, was polarized to ~15% using the dynamic nuclear polarization method (paper IV). The molecule has low toxicity, and it is biologically stable within the time scale of the imaging experiment. The concentration of the dissolved molecule after polarization is approximately 200 mM, and the T_1 in water solution is ~80 s.

Signal expressions for hyperpolarized nuclei

The acquisition of signal from a hyperpolarized substance differs from signal acquisition of thermally polarized spins. For thermally polarized spins, the longitudinal magnetization recovers through T_1 relaxation between each RF pulse. For hyperpolarized spins, however, the effect of T_1 relaxation causes magnetization decay instead of regrowth, and the magnetization eventually decays to an undetectable (thermal) level. Accordingly, existing signal expressions derived for thermally polarized spins are not valid in the hyperpolarized case. New signal expressions were therefore derived for signal from flowing HP nuclei during imaging with a spoiled gradient echo sequence (paper III), and for signal from a stationary HP substance during a trueFISP imaging experiment (paper IV).

Gradient echo signal from flowing HP nuclei

In the derivation of the gradient echo signal expressions for flowing HP nuclei, a perfectly spoiled gradient echo sequence with a repetition time TR, flip angle α, and slice thickness Δx was assumed. Expressions were derived for both plug flow and laminar flow perpendicular through the image slice (paper III).

The total signal, $S_p(\alpha)$, from a plug flow of an HP substance with velocity v through an image slice is the sum of the signal contributions from the parts of the HP substance that have experienced different numbers of RF pulses (Eq. 5).

$$S_p(\alpha) = S_0 \sin\alpha \left[\frac{1}{n} \sum_{i=0}^{N-1} \cos^i\alpha + \left(1 - \frac{N}{n}\right) \cos^N\alpha \right] \quad (5)$$

$n = \Delta x / v\mathrm{TR}$, and S_0 is the maximal achievable signal if the whole magnetization is utilized in

one excitation. S_0 is proportional to $e^{-t/T1}$. To find the optimal flip angle, Eq. 5 was simplified, differentiated and set equal to zero. For small flip angles, this equation can be solved, resulting in Eq. 6.

$$\alpha = k_p\sqrt{\frac{1}{n}} = k_p\sqrt{\frac{vTR}{\Delta x}} \tag{6}$$

$k_p \approx 1.585$ is a dimensionless constant.

For fully developed laminar flow in a circular vessel perpendicular to the image slice, the total signal, $S_l(\alpha)$, was found by integrating over v, the product of the plug flow signal $S_p(v, \alpha)$, and the flow velocity distribution, $f(v)$, of the flowing substance in a cross-section of the vessel (Eq. 7). This expression was verified in flow phantom measurements (section Flow phantom experiments using HP ^{129}Xe).

$$S_l(\alpha) = \int f(v)S_p(v,\alpha)\,\mathrm{d}v \tag{7}$$

From this expression, and with the same approximations as for plug flow, the optimal flip angle for laminar flow was derived (Eq. 8).

$$\alpha = k_l\sqrt{\frac{v_0TR}{\Delta x}} \tag{8}$$

Here, v_0 is the mean flow velocity in the vessel, and $k_l \approx 1.652$ is another dimensionless constant. The expressions for optimal flip angles (Eqs. 6 and 8) were derived using a small flip angle approximation. For higher flip angles, these expressions were verified with simulations of Eqs. 5 and 7.

TrueFISP signal from HP nuclei

In conventional ^{1}H trueFISP MRI, imaging is commonly performed during a signal steady-state reached after a number of RF excitations. For a hyperpolarized substance, however, the effect of the T_1-relaxation is such that a steady-state is not reached until the polarization level, and thereby the signal level, is too low to be useful (i.e., approaching thermal levels). However, if the relaxation times are long compared to the acquisition time, the signal decay is slow enough to allow imaging during this ''pseudo'' steady-state. Assuming stationary spins and no off-resonance effects, an expression for the transversal part of the magnetization, $M_{y,n}$ (i.e., the signal), as a function of the number of excitations, n, was derived (paper IV):

$$M_{y,n} = \sin\frac{\theta}{2}\left(\left(E_1\cos\frac{\theta}{2}\right)^2 + \left(E_2\sin\frac{\theta}{2}\right)^2\right)^{n/2} \tag{9}$$

$E_1 = e^{-TR/T_1}$, and $E_2 = e^{-TR/T_2}$, respectively. Eq. 9 can be used to estimate the signal in an MR image, with n set to the number of RF pulses applied when the central k-space line is encoded. For long relaxation times and a small n, the outer parenthesis in Eq. 9 reduces to 1, and the signal is simply described by $\sin(\theta/2)$.

Flow phantom experiments using HP ^{129}Xe

The theoretical gradient echo signal expressions derived for signal from flowing HP substance (section Gradient echo signal from flowing HP nuclei) were evaluated with flow phantom measurements (paper III). A flow of ethanol was established in a soft PVC tube through the magnet. Three mean flow velocities were used, 14, 21, and 36 cm/s. During each experiment, the dissolved HP ^{129}Xe solution (section Hyperpolarization and preparation of ^{129}Xe and ^{13}C) was injected into the flow system. The flip angle dependency was studied by acquisition of consecutive gradient echo images with different flip angles (10–90°) during bolus passage. In these experiments the flow was oriented ''through plane''. A series of in-plane images were also acquired during passage of a bolus of ^{129}Xe solution with a mean velocity of 18 cm/s.

Phantom experiments using HP ^{13}C

The flip angle dependence for the trueFISP pulse sequence (Eq. 9) and the new HP ^{13}C-based CM was studied experimentally (paper IV). Syringes were filled with the HP ^{13}C-based CM and imaged with different flip angles (10–180°). For comparison, corresponding images were also obtained using a spoiled gradient echo pulse sequence.

The relaxation times of the CM in water solution were estimated (paper IV). T_1 was calculated from two images of two different CM-filled syringes acquired at two different times after the end of the polarization. A mono-exponential T_1-decay between acquisitions was assumed. T_2 was estimated from the signal decay in 15 consecutively acquired images using the trueFISP pulse sequence with the flip-back concept and a flip angle of 180°. Mono-exponential signal decay due to T_2 was assumed in the series.

The T_2 relaxation time of the CM in human blood (CM concentration ≈ 100 mM, thermally polarized) was measured *in vitro* using a 9.4 T NMR magnet (Innova 400, Varian, Palo Alto, USA) and a Carr–Purcell–Meiboom–Gill (CPMG) pulse sequence. Two different interecho times were used, 1 and 5 ms. The measurements of the blood/CM sample

were performed approximately five to 10 min after mixing the CM with the blood.

The trueFISP pulse sequence is normally very sensitive to field inhomogeneities. However, the use of a flip angle of 180° makes the pulse sequence scheme similar to a RARE pulse sequence. In RARE imaging, the 180° pulses refocus the dephasing caused by inhomogeneities. To test whether a trueFISP pulse sequence with high flip angles results in similar effects, a series of phantom images were acquired with different flip angles and an intentionally poorly shimmed magnet. Ordinary tap water was used in the phantom. Water has long relaxation times compared to the acquisition time and acted as a substitute for the HP ^{13}C-substance in this experiment.

In vivo *imaging with the HP ^{13}C-based CM*

A series of CE-MRA experiments were performed in four living anesthetized male Wistar rats (paper IV). HP ^{13}C-based CM (3–3.5 mL) was injected intravenously into the tail vein of the animals. Immediately after injection, imaging was performed with the trueFISP pulse sequence (FA = 180°). Fifteen to 20 consecutive images were obtained using the flip-back concept. In two of the animals the FOV covered the thoracic and abdominal region, and in the other two, the head-neck region was covered. The T_2 relaxation time for the CM *in vivo* was estimated from the total signal decay in one of the image series covering the thoracic and abdominal region (paper IV).

The T_1 relaxation time of the CM *in vivo* was measured in two living but anesthetized female NMRI mice (20–40 g). Mice were chosen due their size, in order to ensure that the whole animal was covered by the coil and hence experienced the excitation pulse. HP CM (0.5 mL) was injected intravenously, and FIDs were acquired every third second after excitation with non-selective RF pulses (FA = 3°). The T_1 was estimated from a mono-exponential fit to the maximum value in each FID acquired.

RESULTS

Effects of a varying CM concentration during 3-D CE-MRA

A varying CM concentration during image acquisition leads to undesired variations in the MR signal. These variations cause problems for the Fourier transform used for image reconstruction and may result in image artifacts, and/or loss of vascular signal (paper I). Simulations showed that a rapid CM concentration variation during encoding of the central parts of *k*-space yields severe image artifacts. A slower, more patient-like concentration variation, corresponding to an intravenous injection of CM, did not result in artifacts, but the vascular signal was degraded if maximum CM concentration did not coincide with sampling of the central parts of *k*-space (Fig. 11).

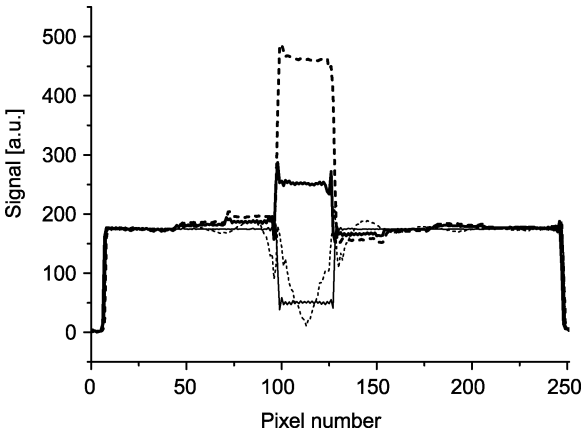

Fig. 11. Line profiles from simulated MR images covering an aorta with surrounding fatty tissue. Without contrast-enhancement, the aortic signal is lower than the surrounding tissue (thin solid line). A patient-like bolus centered in *k*-space yields good contrast-enhancement without artifacts (thick dashed line), whereas a poor timing leads to vascular signal loss (thick solid line). A rapid concentration variation during encoding of the central *k*-space lines causes heavy artifacts and signal loss (thin dashed line).

The 3-D simulation model proved capable of simulating images from a 3-D CE-MRA experiment, taking into account the effects of CM concentration variation and pulsatile flow. However, due to the short TE of the pulse sequence used, the simulated pulsatile aortic blood flow only produced some minor ghost artifacts (paper I).

It was also shown that it is important to include tissue surrounding the vessel in order to display the effects of a CM concentration variation accurately in this kind of simulation.

The results from the simulations were confirmed qualitatively in phantom measurements. The CM bolus centered in *k*-space yielded artifact-free images with good contrast-enhancement, whereas the poorly timed bolus resulted in signal loss and image artifacts.

Flow-induced phase in a 3-D CE-MRA pulse sequence

If flow-induced phase information is to be used for separation of arteries and veins in a CE-MRA image

volume, it is important to avoid phase aliasing. This is assured if the V_{enc} of the pulse sequence is larger than the highest flow velocities present. The linear relationship between phase accumulation and flow velocity in the evaluated 3-D CE-MRA pulse sequence (Eq. 1) was confirmed with flow phantom measurements (paper II). The V_{enc} of the pulse sequence was 74 cm/s. The mean flow velocity over a cardiac cycle in the popliteal artery of a volunteer was measured to be 6 cm/s, and thus corresponds to a phase accumulation of approximately 15° (paper II). Accordingly, the risk of phase aliasing is low, and the phase accumulation was used to separate the arteries from the veins after CE-MRA in the same volunteer (section Post-processing in 3-D CE-MRA: extinguishing veins).

Post-processing in 3-D CE-MRA: extinguishing veins

The postprocessing method described in section Separation of arteries and veins was evaluated in flow phantom experiments, with flow velocities of 9 and 15 cm/s. In both cases, signal from flow in one direction was effectively suppressed, while signal from flow in the opposite direction was unaffected (paper II).

In CE-MRA with extracellular CM in a volunteer, exclusive arterial enhancement was achieved by timing the image acquisition to the first-pass of the bolus in the volume of interest (Fig. 12a). For a later acquisition, both arterial and venous structures were enhanced (Fig. 12b). Similar vascular enhancement is achieved if a blood pool agent is used and the acquisition is performed during equilibrium concentration of the CM in the vessels. The data set in Fig. 12(b) was postprocessed to suppress venous enhancement, and the result after global segmentation is seen in Fig. 12(c) (paper II). Similar results were obtained using local segmentation. In the volunteer experiments with a blood pool agent, the local segmentation method was more successful, possibly due to a failure of the phase subtraction used in global segmentation (paper II).

In the segmented image, major arterial structures are still visible and good venous suppression is achieved. Smaller vessels oriented in the transverse plane are not handled correctly. One possible explanation is that the segmentation algorithm is based on flow in the superior–inferior direction, and not flow in the transverse plane.

This technique for artery-vein separation could potentially be improved, either by increasing the flow sensitivity of the pulse sequence, or by combining it with other methods such as those based on susceptibility differences and/or pure image processing.

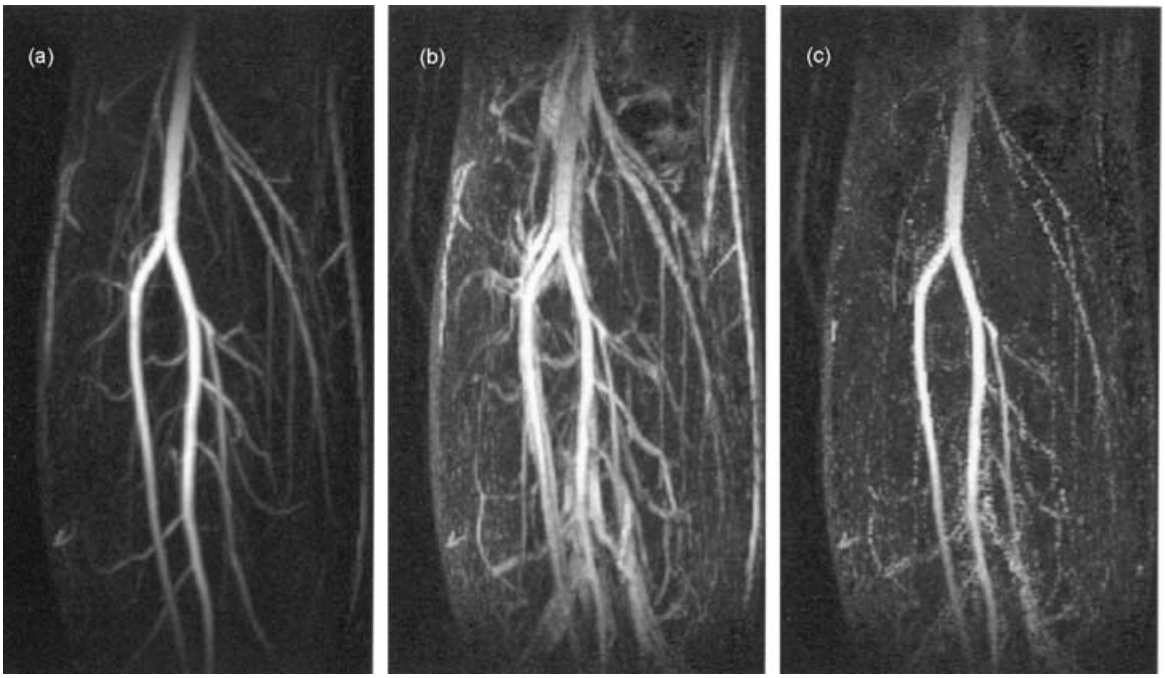

Fig. 12. MIP images from 3-D CE-MRA data sets acquired using different bolus timings of an extracellular CM on a volunteer: (a) acquisition timed to enhance only arterial structures; (b) late acquisition resulting in enhancement of both arteries and veins. After post-processing (global segmentation), most venous structures were removed (c).

Table 1
Measured relaxation times for the ^{13}C-based CM

^{13}C Relaxation time	Measured in	No. meas.	Result [s]
T_1	Water	8	82 ± 6
T_1	*In vivo*, living mouse	2	37.5
T_2	Water[1]	1	18
T_2	*In vitro*, human blood[2]	1	4.0
T_2	*In vitro*, human blood[3]	1	1.6
T_2	*In vivo*, living rat[1]	1	1.3

T_2 relaxation times measured with [1]TrueFISP, TE = 3.6 ms; [2]CPMG, TE = 1 ms; [3]CPMG, TE = 5 ms.

Relaxation times for the HP ^{13}C-based CM

The relaxation times of the new contrast medium based on ^{13}C are long (Table 1). The T_2 especially is extremely long (>1 s), and hence a pulse sequence able to take advantage of this long T_2 should be used for imaging the CM. The values in blood are shorter than those in water solution, but they are still long enough to allow for *in vivo* imaging. The T_2 values measured *in vivo* are probably contaminated by dephasing effects other than pure T_2, and should be seen as a worst-case estimation of the true *in vivo* T_2 value (paper IV). Furthermore, the difference in the two T_2 values measured in human blood *in vitro* indicate that the T_2 is dependent of the TE used for measurement. However, for the short TE typically used in fast imaging (1–5 ms), the T_2 value for the CM in blood appears to be in the order of 1–4 s.

Inflow effects in gradient echo imaging of a flowing HP substance

The derived expressions for optimal flip angle and highest achievable signal agreed well with numerical evaluation of the signal expressions for varying flip angle and flow velocity. Evaluating Eq. 7 for a through plane laminar flow distribution of an HP substance gives an optimal flip angle which increases with increasing flow velocity (paper III). This relationship was verified with phantom measurements at three different flow velocities. The measured data agreed well with theoretical calculations (Fig. 13). The optimal flip angle for HP flowing nuclei is smaller than for thermally polarized flowing nuclei with short T_1 (e.g., contrast-enhanced blood). This difference decreases with increasing flow velocity (paper III).

Signal from an HP substance obtained with a trueFISP pulse sequence

For long relaxation times and for small imaging matrices, Eq. 9 is closely approximated by $\sin(\theta/2)$,

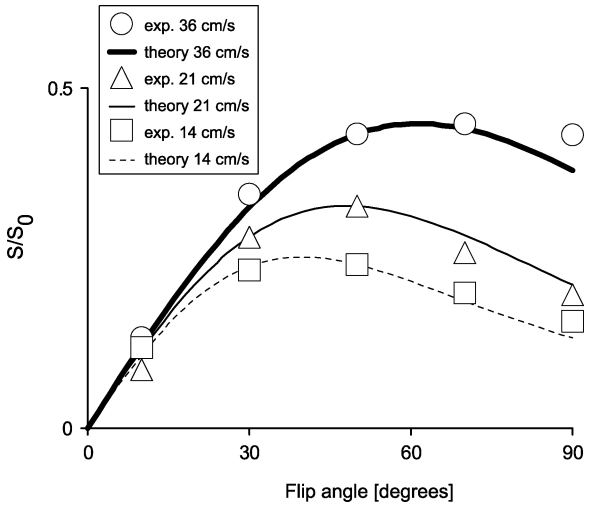

Fig. 13. Experimental and theoretical signal dependency on flip angle for three different flow velocities of HP ^{129}Xe dissolved in ethanol, imaged with a spoiled gradient echo sequence (slice thickness = 10 mm, TR = 12 ms) (paper III). $S/S_0 = 1$ corresponds to the maximal signal from a single 90° RF excitation.

and the optimal flip angle is 180° (Fig. 14). This was confirmed in phantom experiments with the ^{13}C-based HP CM in water solution, and a 64×64 matrix (paper IV). The corresponding calculations with Eq. 9 were evaluated for 32 pulses, i.e., the number of experienced pulses when the central *k*-space line is encoded in a sequentially encoded 64×64 matrix.

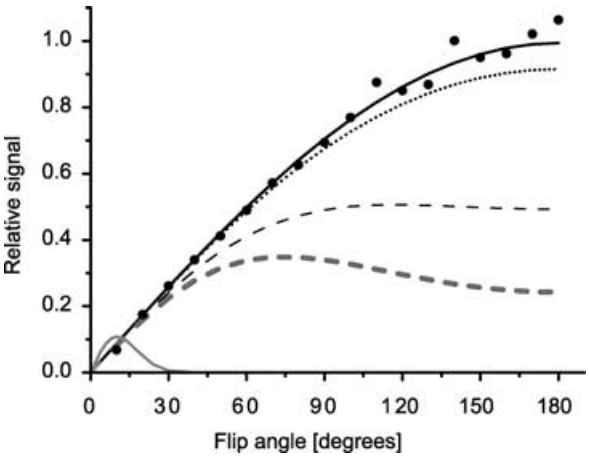

Fig. 14. Calculated signal for the HP ^{13}C-based CM in water solution obtained with a trueFISP pulse sequence after 32 pulses (solid black line). These values agree well with measured data (circles). Calculated signal values are also plotted for the CM *in vivo* after 32 pulses (black dotted line), 256 pulses (black dashed line), and 512 pulses (gray dashed line). For comparison, the corresponding theoretical signal for a FLASH pulse sequence after 32 pulses is also plotted (solid gray line). Measured and calculated data are normalized at FA = 70°.

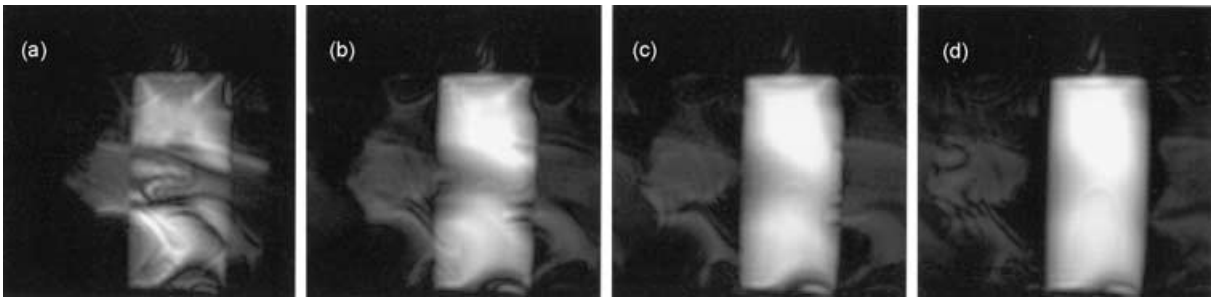

Fig. 15. TrueFISP images of a water phantom acquired with a poor shim and different flip angles: (a) 60°, (b) 120°, (c) 150°, (d) 180°. At low-flip angles the trueFISP pulse sequence is very sensitive to field inhomogeneities, but higher flip angles act refocusing and compensate for this effect.

The relaxation times of the CM *in vivo* are shorter than in water solution (section Relaxation times for the HP ^{13}C-based CM), but they are still long enough to result in an optimal flip angle of 180° for a small imaging matrix. If larger matrices are used, the larger number of applied RF pulses decreases the ^{13}C-signal in the image. The optimal flip angle also decreases with increasing number of RF pulses applied, since T_2 is always shorter than T_1 (Fig. 14).

In a FLASH pulse sequence, the transverse magnetization is spoiled between each excitation, and the long relaxation times of the CM are not utilized. Accordingly, the maximum obtainable FLASH signal is much lower than the maximal signal from a trueFISP pulse sequence. This was confirmed with phantom experiments (paper IV), and for the parameters used, the FLASH signal was lower than the trueFISP signal by a factor nine.

The sensitivity of the trueFISP pulse sequence to magnetic field inhomogeneities was evaluated in experiments with an intentionally poorly shimmed magnet and a water phantom (Fig. 15). The water with its long relaxation times acted as substitute for the HP ^{13}C-substance. At low flip angles the sequence is very sensitive to inhomogeneities, and the images contain heavy artifacts. For higher flip angles, however, the refocusing property of the RF pulses becomes more discernible, and with a 180° flip angle the images are in principle artifact-free.

CE-MRA with the HP ^{13}C-based CM

The HP ^{13}C-based CM can be used for contrast-enhanced MRA with high SNR in living rats (paper IV). Angiograms with good visualization of the vascular structures (e.g., vena cava, aortic arc, aorta, renal arteries, common carotid arteries, and the external jugular veins) were obtained (Fig. 16). SNR in vena

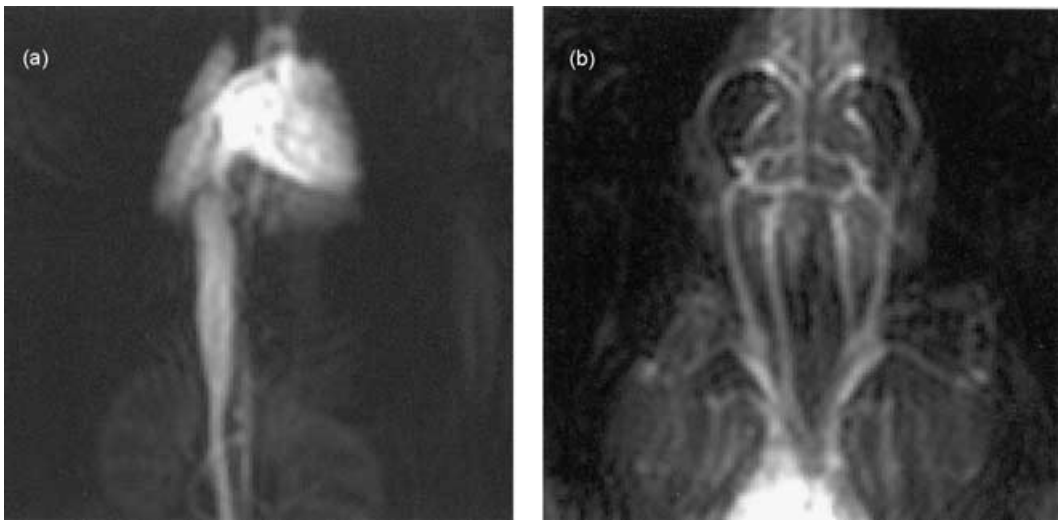

Fig. 16. Two angiograms from CE-MRA experiments with the HP ^{13}C-based CM in living rats. The images cover the thoracic and abdominal region (a), and the head-neck region (b).

cava was measured to 240, and in the highly enhanced cardiac and pulmonary region SNR was approximately 500. In a small region within the carotid arteries, SNR was measured to be ∼75 (paper IV).

The hyperpolarized CM results in a very high contrast-to-noise ratio (CNR). In the acquired angiograms, all of the signal originates from the HP ^{13}C-nuclei and as long as the CM stays in the vascular space, enhancement of surrounding tissue is minimal (paper IV).

The long T_2 of the CM together with the flip-back concept make it possible to preserve signal from one image acquisition to the next. In a series of 15 consecutively acquired images, an SNR of 500 in the cardiac region of the first image decayed to 260 in the fourth, and to approximately 10 in the last image (paper IV).

A rough estimation of the distribution of the CM over time was obtained by following the signal variation in three different regions in an image series containing 20 images, corresponding to a total time of 4.6 s (Fig. 17). Since a 180° flip angle was used, signal was assumed to decay through T_2 relaxation only, independently of T_1. All signal values were therefore corrected using the estimated T_2 of 1.3 s (section Relaxation times for the HP 13C-based CM). The initially high signal in the cardiac region indicates that the first images are acquired during first-pass of the CM in this region. The declining cardiac signal in the following images is due to the CM being distributed to the whole blood pool. This is further supported by the vena cava signal, which initially falls, but then recovers to levels similar to the cardiac signal in the last images. In the kidneys, however, the signal increases constantly through the image series. This could be a first indication of a fast biodistribution of the CM. The results are very preliminary, and the signal is only followed for 4.6 s, which is too short a time for estimation of important parameters such as vascular half-life of this new CM.

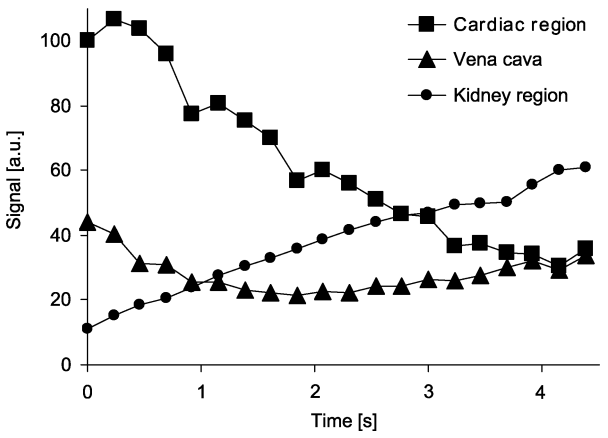

Fig. 17. Signal variation due to biodistribution in three different regions in the CE-MRA images obtained using the HP ^{13}C CM. All signal values are corrected for T_2-decay during imaging.

DISCUSSION

Following the work of Prince *et al*. (99, 102), CE-MRA has now developed into a valuable clinical tool for diagnosing vascular disease. The short acquisition times together with the fact that the technique can be used regardless of blood flow and vessel orientation has made vascular MR imaging possible in many parts of the body, e.g., the abdominal aorta and the renal arteries (112, 126), the pulmonary vessels (84, 127), the carotid arteries (59, 119), and the peripheral vessels (51).

At present, clinical CE-MRA is performed using extracellular Gd-based CM with short vascular half-life. Imaging must therefore be performed during first-pass of the CM in the vessels in order to ensure a high vascular SNR and CNR. Poor bolus timing or a very fast injection might lead to image artifacts (paper I). This is not a problem solely for the extracellular CM but is a general problem when performing CE-MRA during the first-pass, regardless of the type of CM used. The short time window of peak CM enhancement for extracellular CM has, however, caused an increased interest in new types of contrast medium.

A blood pool type of CM might seem to be the agent of choice for CE-MRA. The larger molecular sizes lead to higher relaxivity, and accordingly a high SNR can be achieved with lower doses than with the extracellular CM of today. The blood pool property also extends the acquisition time window, enabling higher spatial resolution, and the use of, e.g., cardiac triggering, navigator techniques and acquisition averaging. However, imaging during CM concentration equilibrium inevitably leads to simultaneous enhancement of arterial and venous structures. Hence, the success of future blood pool agents in CE-MRA depends on the development of fast and reliable methods for artery/vein separation. Several methods have been proposed. Some of them are based on the physical properties of the contrast-enhanced blood (paper II, 8, 30, 131); others are based on differences in temporal enhancement patterns of the two vessel types (9, 21, 54, 82, 83, 111), or on pure image processing techniques (66, 116, 122). The most general of these different approaches

are the ones based solely on image processing, in that they do not depend on physical or physiological properties of the blood, nor on specialized acquisition protocols. These methods do however, require a high spatial resolution, a condition that presumably can be met by the longer acquisition times made available through the use of a blood pool agent.

The recent development of techniques for hyperpolarizing certain nuclei and utilizing them as a new type of contrast medium (paper III, paper IV) is an exciting approach for increasing the SNR in MR angiography. Under certain circumstances, a higher SNR can be traded for shorter acquisition times or increased spatial resolution. This would enable or improve imaging of fast-moving structures such as the coronaries, or vessels with a short time of exclusive arterial enhancement such as the carotids or the intracranial vessels. For a CM based on hyperpolarized nuclei to be successful, it must be able to yield a higher SNR than what is possible with current proton-based techniques. It is thus of interest to compare the achievable SNR for HP-based CM with SNR in conventional MRI.

If the predominant source of noise in an MR experiment is the sample (which is true in most practical cases) (26), the maximum achievable SNR at a given field strength is proportional to the product of the gyromagnetic ratio (γ), the polarization (P) and the concentration of the nuclei used. In Table 2, these parameters are listed for ^{1}H in blood, and for possible CM based on HP nuclei. In CE-MRA with a conventional CM, signal is obtained from the thermally polarized protons in blood (polarization $\sim 5 \times 10^{-6}$ at 1.5 T, concentration $\sim$80 M), whereas the signal from an HP CM is obtained directly from the hyperpolarized nuclei. The polarizations listed for ^{129}Xe, ^{3}He and ^{13}C are levels routinely achievable today (paper IV, 88). The concentration for an HP CM *in vivo* depends on the concentrations injected. For ^{129}Xe-gas, the delivered concentration is limited by the solubility (the Ostwald coefficient) of the gas in blood or in the carrier used. The listed value is based on ^{129}Xe of natural abundance (26.4%) dissolved in a hypothetical carrier with an Ostwald coefficient of 1. The Ostwald coefficient for xenon in pure blood is much lower, approximately 0.17 (93). For ^{3}He-gas encapsulated in microbubbles, the concentration depends on the concentration and size of the bubbles in the carrier suspension (12, 17). The HP ^{13}C-nucleus is part of a water-soluble molecule, and the deliverable concentration is in this case only limited by the concentrations that can be reached during the polarization procedure (paper IV). Apart from the concentration injected, there is also an inevitable dilution of the CM on its way to the vessel of interest (Table 2). For the cardiac output of a standard man (5 L/min), and a fast bolus injection (7 mL/s), this dilution factor is approximately 12 (65). For xenon, there is an extra factor of five due to ventilation of the xenon gas during passage through the pulmonary system (65).

Table 2
Parameters of interest for SNR comparison, listed for different nuclei. The relative SNR values ($\gamma \times p \times$ Conc./dilution) are normalized to yield 100 for ^{1}H

	^{1}H	^{129}Xe	^{3}He	^{13}C
γ [MHz/T]	42.6	11.7	32.5	10.7
P	5×10^{-6}	0.2	0.3	0.15
Conc. [M]	80	0.01	0.002	0.2
Dilution factor	1	60	12	12
Relative SNR	100	2.3	9.5	157

See text for information on the different parameters.

With these parameters, the maximum achievable SNR for CM based on HP gas (^{129}Xe, ^{3}He) is at least one order of magnitude less than for conventional CM. Xenon can also be delivered through inhalation, with a maximal arterial concentration of approximately 0.26 mM (78). This corresponds to a similar signal level as for intravenously injected xenon (relative SNR = 3.6). Accordingly, these nuclei are not suitable for MRA with the present concentrations and polarizations. The SNR for ^{13}C-based and conventional CM are however, comparable. Furthermore, the polarization level listed for ^{13}C is obtained with a prototype polarizer. The technique is still under development and improvements in both concentration and polarization level of ^{13}C in the suggested CM can be expected to increase the SNR achievable by at least one order of magnitude.

In the comparison above, the full magnetization is assumed to be used for image formation. However, CE-MRA with a conventional CM is performed with spoiled gradient echo sequences and relatively small flip angles, utilizing only a fraction of the available magnetization. The suggested ^{13}C-based CM, on the other hand, has an extremely long T_2 (>1 s, *in vivo*), and hence acquisition techniques able of utilizing almost all of the available magnetization can be used (paper IV). Summarizing the factors discussed, it is clear that the suggested HP CM based on ^{13}C have a potential to increase the achievable SNR of CE-MRA.

Not only the vascular signal, but also the blood-tissue contrast is of great importance in achieving a clinically valuable angiogram. With a conventional CM, the difference in contrast between enhanced

blood and the surrounding tissue is a consequence of different signal saturation of the two tissues. For an HP CM administered solely to the vascular space, however, the signal from surrounding tissue is practically zero, creating a huge blood-tissue contrast. If the HP CM is not retained in the blood pool, imaging must be performed during first-pass in order to take advantage of this effect. The preliminary results in section CE-MRA with the HP ^{13}C-based CM indicate that this is the case for the new ^{13}C-based HP CM studied in paper IV. Even if it were possible to develop a blood pool agent based on HP nuclei, it might not be very applicable. The advantage of the blood pool property is that it allows longer acquisition times during CM concentration equilibrium. An HP-based CM has an inherent restriction in maximal acquisition time due to the effect of relaxation *in vivo*. The T_1 has to be long enough to allow imaging after the CM has reached equilibrium concentration instead of during first-pass. The limited amount of available magnetization in an HP substance also restricts the total number of excitations and the total acquisition time. If these requirements can be fulfilled, the HP blood pool agent will not be different from paramagnetic blood pool agents, i.e., the acquired data must be post-processed to separate arteries from veins. Most of the separation methods suggested for paramagnetic CM should, however, be applicable to HP CM also.

The absence of signal in non-vascular tissue may also be used for new image acquisition techniques. With a conventional CM the standard method is to acquire a 3-D volume, and use post-processing techniques such as MIP to visualize the vascular structure. However, with an HP CM, acquisition of a single thick 2-D slice covering the volume of interest can be used to produce an MIP-like image. Even though this 2-D MIP cannot be reformatted to other viewing angles, the shorter acquisition time as compared with conventional techniques is in some applications (e.g., for time-resolved MRA) more important than the full 3-D information. Another general advantage of a short acquisition time is that CM concentration variation during imaging is smaller. This reduces the risk of image artifacts (paper I).

The rapid development of MR scanner hardware has of course contributed to the success of CE-MRA in general. The use of stronger gradients and multiple coils has enabled short acquisition times of image volumes covering large segments of the body. The current development of parallel imaging techniques is an interesting way of further reducing the total acquisition time in MR imaging. With this technique multiple simultaneously operating receiver coils are used to accelerate data acquisition. The difference in spatial sensitivity for the different coils is used to reduce the total number of excitations needed to produce an MR image. In sensitivity encoding (SENSE), a reduced FOV image is acquired simultaneously with each coil element. These images can then be ''unfolded'' to one full FOV image with knowledge of each coil's spatial sensitivity (103). In simultaneous acquisition of spatial harmonics (SMASH), linear combinations of the different coil sensitivities are used to derive missing phase encoding lines in an under-sampled *k*-space (114). These methods have already been applied to conventional CE-MRA with a reduction in total acquisition time of a factor of two or more (36, 75, 115, 132). The reduction in acquisition time in parallel imaging is at the expense of SNR to some extent. Accordingly, a CM able to yield a high SNR would be useful to make the most of this technique. The CM based on HP ^{13}C evaluated in this thesis could be a candidate for fulfilling this requirement.

The strong and fast gradients in modern MR scanners are also a must for future use of an HP CM based on nuclei with low γ (such as ^{13}C). A low γ leads to a corresponding increase in the gradient strength needed to produce an image with a certain FOV. Thus, in the pulse sequences used, weak gradients prolong the shortest possible TR, and thereby the total acquisition time.

Despite the great future potential of the new contrast media currently under development, the ease of use and robustness of conventional extracellular CM remains. Even if an HP CM with extraordinary signal properties is developed, it will be subject to problems similar to those attributed to conventional CM, e.g., injection timing or simultaneous arterial and venous enhancement. It is therefore likely that CE-MRA with conventional CM will continue to be the predominant technique in those parts of the body where it is successfully used today. However, as discussed above, a higher SNR and/or shorter acquisition times would be very useful for CE-MRA of some vascular structures. In those regions the future blood pool agents and hyperpolarized CM most certainly have the potential to become the optimal choice.

FUTURE ASPECTS

CE-MRA with paramagnetic CM is a valuable clinical tool in diagnosing vascular disease. One way of improving the present techniques further is through increased vascular SNR. Development of new types

of CM, e.g., based on HP substances, can contribute to this.

Below is a list of suggestions for future study in the field of CE-MRA:

- Development of the 3-D simulation model used in Paper I to be used in studies of hyperpolarized nuclei. The model is general and could be a valuable and fast tool in evaluation of new pulse sequence techniques and in comparisons between conventional and hyperpolarized CM.
- Combining the artery-vein separation method used in Paper II with other suggested separation techniques, such as those based on susceptibility differences and/or vessel tracking algorithms. The success of future blood pool agents depends on a technique capable of separating arteries from veins accurately, and today no established method exists.
- Performing studies on the trueFISP pulse sequence used in Paper IV. The behavior of the signal from a trueFISP pulse sequence in the presence of flow is yet to be evaluated. Furthermore, the use of a large flip angle makes trueFISP very similar to a RARE pulse sequence, and an interesting task would be to study the differences and the similarities between the two pulse sequences in terms of, e.g., T_2/T_2^*-weighting and sensitivity to field inhomogeneities.
- Application of parallel imaging techniques in imaging of HP substances. A high SNR from an HP CM can be traded for shorter imaging times using parallel imaging techniques.
- Performing studies on the biodistribution of the HP ^{13}C CM tested in Paper IV. It is important to gain knowledge of how fast it leaves the vascular compartment, and how it is excreted.
- Evaluation of the usefulness of the HP ^{13}C CM in other types of study, e.g., for quantitative perfusion.

CONCLUSIONS

Studies were performed on contrast-enhanced magnetic resonance angiography using both paramagnetic CM and a new type of CM based on HP nuclei.

If CE-MRA is performed during first-pass of a CM in the vessels of interest, it is important that peak concentration of the CM coincides with encoding of the central parts of *k*-space, in order to maximize vascular enhancement. Furthermore, a rapid concentration variation during encoding of the central *k*-space lines can result in severe image artifacts (paper I).

Simultaneous enhancement of arteries and veins may cause problems in separating them in angiograms. These problems can be reduced by the use of a postprocessing method able to extinguish venous signal, while leaving arterial signal unchanged. Such a method was developed and used successfully in larger vascular structures in the lower leg of volunteers (paper II). Smaller vessels not directed superior-inferior, were however, not correctly handled.

The possibility of using hyperpolarized nuclei as a new type of contrast medium for CE-MRA was evaluated (paper III, paper IV). The signal from flowing HP nuclei during imaging with a spoiled gradient echo sequence was studied theoretically, and signal expressions were derived. The theory was confirmed in a phantom model using HP ^{129}Xe dissolved in ethanol (paper III).

The first tests of HP ^{13}C as a CM for CE-MRA in living rats were performed (paper IV). Angiograms with high SNR were obtained by combining the high polarization and high concentration of ^{13}C in a water-soluble molecule with an optimized trueFISP pulse sequence.

CE-MRA with paramagnetic CM is a valuable diagnostic tool. However, through the development of new types of CM, e.g., based on HP ^{13}C, it may be possible to increase the signal levels achievable in CE-MRA further

ACKNOWLEDGMENTS

This work was in part supported by grants from Region Skåne, through '*Hälso- och sjukvårdsförvaltningens donations-fonder och stiftelser*', and '*Landstingsfinansierad regional forskning*'. Amersham Health R&D AB is acknowledged for their support in the research on hyperpolarized nuclei.

REFERENCES

1. ALBERT M. S., CATES G. D., DRIEHUYS B., et al.: Biological magnetic resonance imaging using laser-polarized ^{129}Xe. Nature 370 (1994), 199.
2. ALFIDI R. J., MASARYK T. J., HAACKE E. M., et al.: MR angiography of peripheral, carotid, and coronary arteries. Am. J. Roentgenol. 149 (1987), 1097.
3. ANZAI Y., PRINCE M. R., CHENEVERT T. L., et al.: MR angiography with an ultrasmall superparamagnetic iron oxide blood pool agent. J. Magn. Reson. Imaging 7 (1997), 209.
4. BACHERT P., SCHAD L. R., BOCK M., et al.: Nuclear magnetic resonance imaging of airways in humans with use of hyperpolarized ^{3}He. Magn. Reson. Med. 36 (1996), 192.
5. BECKER J., BERMUTH J., EBERT M., et al.: Interdisciplinary experiment with polarized ^{3}He. Nucl. Instrum. Meth. Phys. Res. A. 402 (1998), 327.
6. BIFONE A., SONG Y. Q., SEYDOUX R., et al.: NMR of laser-polarized xenon in human blood. Proc. Natl. Acad. Sci. U.S.A. 93 (1996), 12932.

7. BJÖRNERUD A. & MYHR G. MR-kontrastmidler – virkningsmekanismer. In: Fokus På MRI Og Bruk Av Kontrastmidler. Edited by G. MYHR, K. NORDLID, A. BJÖRNERUD, & E. G. LIHAUG.: Nycomed Imaging, AS, Oslo 1996, p. 42.
8. BLUEMKE D. A., DARROW R. D., GUPTA R., TADIKONDA S. K. & DOMOULIN C. L.: 3D contrast enhanced phase contrast angiograhy: utility for arterial/venous segmentation. Proceedings of the International Society for Magnetic Resonance in Medicine, 7th Scientific Meeting, Philadelphia, USA 1999, p. 1237.
9. BOCK M., SCHOENBERG S. O., FLOEMER F. & SCHAD L. R.: Separation of arteries and veins in 3D MR angiography using correlation analysis. Magn. Reson. Med. 43 (2000), 481.
10. BOSMANS H., WILMS G., DYMARKOWSKI S. & MARCHAL G.: Basic principles of MRA. Eur. J. Radiol. 38 (2001), 2.
11. CALLOT V., CANET E., BROCHOT J., et al.: Vascular and perfusion imaging using encapsulated laser-polarized helium. MAGMA 12 (2001a), 16.
12. CALLOT V., CANET E., BROCHOT J., et al.: MR perfusion imaging using encapsulated laser-polarized ^{3}He. Magn. Reson. Med. 46 (2001b), 535.
13. CARROLL T. J.: The emergence of time-resolved contrast-enhanced MR imaging for intracranial angiography. AJNR Am. J. Neuroradiol. 23 (2002), 346.
14. CARROLL T. J., KOROSEC F. R., SWAN J. S., GRIST T. M., FRAYNE R. & MISTRETTA C. A.: Method for rapidly determining and reconstructing the peak arterial frame from a time-resolved CE-MRA exam. Magn. Reson. Med. 44 (2000), 817.
15. CARROLL T. J., KOROSEC F. R., SWAN J. S., HANY T. F., GRIST T. M. & MISTRETTA C. A.: The effect of injection rate on time-resolved contrast-enhanced peripheral MRA. J. Magn. Reson. Imaging 14 (2001), 401.
16. CHAKERES D. W., SCHMALBROCK P., BROGAN M., YUAN C. & COHEN L.: Normal venous anatomy of the brain: demonstration with gadopentetate dimeglumine in enhanced 3-D MR angiography. Am. J. Roentgenol. 156 (1991), 161.
17. CHAWLA M. S., CHEN X. J., COFER G. P., et al.: Hyperpolarized ^{3}He microspheres as a novel vascular signal source for MRI. Magn. Reson. Med. 43 (2000), 440.
18. CHAWLA M. S., CHEN X. J., MOLLER H. E., et al.: *In vivo* magnetic resonance vascular imaging using laser-polarized ^{3}He microbubbles. Proc. Natl. Acad. Sci. U.S.A. 95 (1998), 108325.
19. CREASY J. L., PRICE R. R., PRESBREY T., GOINS D., PARTAIN C. L., KESSLER R. M.: Gadolinium-enhanced MR angiography. Radiology 175 (1990), 280.
20. DEIMLING M. & HEID O.: Magnetization prepared TrueFISP imaging. Proceedings Society of Magnetic Resonance, Scientific Meeting. San Fransisco, USA 1994, p. 495.
21. DU J., MAZAHERI Y., CARROLL T. J., ESPARSA COSS E., GRIST T. M., MISTRETTA C. A.: International Society for Magnetic Resonance in Medicine, 8th Scientific Meeting, Denver, USA 2000, p. 1807.
22. DUHAMEL G., CHOQUET P., GRILLON E., et al.: Xenon-129 MR imaging and spectroscopy of rat brain using arterial delivery of hyperpolarized xenon in a lipid emulsion. Magn. Reson. Med. 46 (2001), 208.
23. DUMOULIN C. L.: Phase–contrast magnetic resonance angiography. Neuroimag. Clin. North Am. 2 (1992), 657.
24. DUMOULIN C. L. & HART H. R. JR: Magnetic resonance angiography. Radiology 161 (1986), 717.
25. EARLS J. P., ROFSKY N. M., DECORATO D. R., KRINSKY G. A. & WEINREB J. C.: Breath-hold single-dose gadolinium-enhanced three-dimensional MR aortography: usefulness of a timing examination and MR power injector. Radiology 201 (1996), 705.
26. EDELSTEIN W. A., GLOVER G. H., HARDY C. J. & REDINGTON R. W.: The intrinsic signal-to-noise ratio in NMR imaging. Magn. Reson. Med. 3 (1986), 604.
27. ENGELBRECHT M. R., SAEED M., WENDLAND M. F., CANET E., OKSENDAL A. N. & HIGGINS C. B.: Contrast-enhanced 3D-TOF MRA of peripheral vessels: intravascular versus extracellular MR contrast media. J. Magn. Reson. Imaging 8 (1998), 616.
28. FELMLEE J. P. & EHMAN R. L.: Spatial presaturation. a method for suppressing flow artifacts and improving depiction of vascular anatomy in MR imaging. Radiology 164 (1987), 559.
29. FISCHER H. & LADEBECK R.: Echo-Planar Imaging Image Artifacts. In: Echo Planar Imaging – Theory, Technique and Application. Edited by F. SCHMITT, M. K. STEHLING & R. TURNER. Springer-Verlag, Heidelberg, Berlin 1998, p. 192.
30. FOO T. K., HO V. B., HOOD M. N. et al.: International Society for Magnetic Resonance in Medicine, 7th Scientific Meeting. Philadelphia, USA 1999, p. 2182.
31. FOO T. K., SARANATHAN M., PRINCE M. R. & CHENEVERT T. L.: Automated detection of bolus arrival and initiation of data acquisition in fast, three-dimensional, gadolinium-enhanced MR angiography. Radiology 203 (1997), 275.
32. FRITZ HANSEN T., ROSTRUP E., LARSSON H. B., SONDERGAARD L., RING P. & HENRIKSEN O.: Measurement of the arterial concentration of Gd-DTPA using MRI. a step toward quantitative perfusion imaging. Magn. Reson. Med. 36 (1996), 225.
33. GAO J. H., HOLLAND S. K. & GORE J. C.: Nuclear magnetic resonance signal from flowing nuclei in rapid imaging using gradient echoes. Med. Phys. 15 (1988), 809.
34. GAO J. H., LEMEN L., XIONG J., PATYAL B. & FOX P. T.: Magnetization and diffusion effects in NMR imaging of hyperpolarized substances. Magn. Reson. Med. 37 (1997), 153.
35. GENTILE T. R., JONES G. L., THOMPSON A. K., et al.: Demonstration of a compact compressor for application of metastability-exchange optical pumping of ^{3}He to human lung imaging. Magn. Reson. Med. 43 (2000), 290.
36. GOLAY X., BROWN S. J., ITOH R. & MELHEM E. R.: Time-resolved contrast-enhanced carotid MR angiography using sensitivity encoding (SENSE). Am. J. Neuroradiol. 22 (2001), 1615.
37. GOLMAN K., ARDENKJAER-LARSEN J. H., SVENSSON J., et al.: ^{13}C-Angiography. Acad. Radiol. 9 (2002), S507.
38. GOLMAN K., AXELSSON O., JOHANNESSON H., MANSSON S., OLOFSSON C. & PETERSSON J. S.: Parahydrogen-induced polarization in imaging: subsecond (13) C angiography. Magn. Reson. Med. 46 (2001), 1.
39. GOYEN M., RUEHM S. G. & DEBATIN J. F.: MR-angiography. the role of contrast agents. Eur J. Radiol. 34 (2000), 247.
40. GRIST T. M., KOROSEC F. R., PETERS D. C., et al.: Steady-state and dynamic MR angiography with MS-325: initial experience in humans. Radiology 207 (1998), 539.

41. GRIST T. M., SPROAT I. A., KENNEL T. W., KOROSEC F. R. & SWAN J. S.: MR angiography of the renal arteries during a breath-hold using gadolinium-enhanced 3D TOF with *k*-space zero-filling and a contrast timing scan. Proceedings International Society for Magnetic Resonance in Medicine, 4th Annual Meeting, New York, USA 1996.
42. GULLBERG G. T., WEHRLI F. W., SHIMAKAWA A. & SIMONS M.: A.: MR vascular imaging with a fast gradient refocusing pulse sequence and reformatted images from transaxial sections. Radiology 165 (1987), 241.
43. HAACKE E. M., BROWN R. W., THOMPSON M. R. & VENKATESAN R.: Magnetic Resonance Imaging, Physical Principles and Sequence Design. John Wiley & Sons, New York, USA 1999.
44. HAACKE E. M., MASARYK T. J., WIELOPOLSKI P. A., et al.: Optimizing blood vessel contrast in fast three-dimensional MRI. Magn. Reson. Med. 14 (1990), 202.
45. HANY T. F., MCKINNON G. C., LEUNG D. A., PFAMMATTER T. & DEBATIN J. F.: Optimization of contrast timing for breath-hold three-dimensional MR angiography. J. Magn. Reson. Imaging 7 (1997), 551.
46. HAUSMANN R., LEWIN J. S. & LAUB G.: Phase-contrast MR angiography with reduced acquisition time: new concepts in sequence design. J. Magn. Reson. Imaging 1 (1991), 415.
47. HENDRICK R. E. & HAACKE E. M.: Basic physics of MR contrast agents and maximization of image contrast. J. Magn. Reson. Imaging 3 (1993), 137.
48. HENNIG J., NAUERTH A. & FRIEDBURG H.: RARE imaging: a fast imaging method for clinical MR. Magn. Reson. Med. 3 (1986), 823.
49. HENNIG J., SCHEFFLER K., LAUBENBERGER J. & STRECKER R.: Time-resolved projection angiography after bolus injection of contrast agent. Magn. Reson. Med. 37 (1997), 341.
50. HIMM J. F.: The Solubility of Xenon in Simple Organic Solvents and in Aqueous Amino Acid Solutions, PhD Thesis. Michigan State University, USA 1986.
51. HO K. Y., LEINER T. & VAN ENGELSHOVEN J. M.: MR angiography of run-off vessels. Eur. Radiol. 9 (1999a), 1285.
52. HO V. B., CHOYKE P. L., FOO T. K., et al.: Automated bolus chase peripheral MR angiography. initial practical experiences and future directions of this work-in-progress. J. Magn. Reson. Imaging 10 (1999b), 376.
53. ITO K., KATO J., OKADA S. & KUMAZAKI T.: K-space filter effect in three-dimensional contrast MR angiography. Acta Radiol. 38 (1997), 173.
54. KAANDORP D. W., KOPINGA K. & WIJN P. F.: Venous signal suppression in 3D dynamic Gd-enhanced carotid artery imaging using the eigenimage filter. Magn. Reson. Med. 42 (1999), 307.
55. KELLER P. J., DRAYER B. P., FRAM E. K., WILLIAMS K. D., DUMOULIN C. L. & SOUZA S. P.: MR angiography with two-dimensional acquisition and three-dimensional display. Work in progress. Radiology 173 (1989), 527.
56. KLISCH J., STRECKER R., HENNIG J. & SCHUMACHER M.: Time-resolved projection MRA. clinical application in intracranial vascular malformations. Neuroradiology 42 (2000), 104.
57. KNOPP M. V., VON TENGG-KOBLIGK H., FLOEMER F. & SCHOENBERG S. O.: Contrast agents for MRA. future directions. J. Magn. Reson. Imaging 10 (1999), 314.
58. KOROSEC F. R., FRAYNE R., GRIST T. M. & MISTRETTA C. A.: Time-resolved contrast-enhanced 3D MR angiography. Magn. Reson. Med. 36 (1996), 345.
59. KOROSEC F. R., TURSKI P. A., CARROLL T. J., MISTRETTA C. A. & GRIST T. M.: Contrast-enhanced MR angiography of the carotid bifurcation. J. Magn. Reson. Imaging 10 (1999), 317.
60. KOUWENHOVEN M. & CONTRAST-ENHANCED M. R.: Angiography, methods, limitations and possibilities. *Acta Radiol*. Suppl. 38 (1997), 57.
61. KROFT L. J. & DE ROOS A.: Blood pool contrast agents for cardiovascular MR imaging. J. Magn. Reson. Imaging 10 (1999), 395.
62. LAUB G. & PURDY D. E.: Variable Tip-angle Slab Selection for improved three dimensional MR Angiography. Proceedings Society of Magnetic Resonance Imaging. New York, USA 1992, p. 167.
63. LAUB G. A. & KAISER W. A.: MR angiography with gradient motion refocusing. J. Comput. Assist. Tomogr. 12 (1988), 377.
64. LAUFFER R. B., PARMELEE D. J., DUNHAM S. U., et al.: MS-325: albumin-targeted contrast agent for MR angiography. Radiology 207 (1998), 529.
65. LAVINI C., PAYNE G. S., LEACH M. O. & BIFONE A.: Intravenous delivery of hyperpolarized (129) Xe: a compartmental model. NMR Biomed. 13 (2000), 238.
66. LEI T., UDUPA J. K., SAHA P. K. & ODHNER D.: Artery-vein separation via MRA – an image processing approach. IEEE Trans. Med. Imaging 20 (2001), 689.
67. LENZ G. W., HAACKE E. M., MASARYK T. J. & LAUB G.: In-plane vascular imaging. pulse sequence design and strategy. Radiology 166 (1988), 875.
68. LIHAUG E. G.: MR-kontrastmidler – utivikling, oversikt, egenskaper. In: Fokus På MRI Og Bruk Av Kontrastmidler. Edited by G. MYHR, K. NORDLID, A. BJÖRNERUD & E. G. LIHAUG. Nycomed Imaging AS, Oslo 1996, p. 56.
69. LIN W., HAACKE E. M., SMITH A. S. & CLAMPITT M. E.: Gadolinium-enhanced high-resolution MR angiography with adaptive vessel tracking: preliminary results in the intracranial circulation. J. Magn. Reson. Imaging 2 (1992), 277.
70. LISTERUD J., EINSTEIN S., OUTWATER E. & KRESSEL H. Y.: First principles of fast spin echo. Magn. Reson. Q 8 (1992), 199.
71. LJUNGGREN S.: A simple graphical representation of fourier-based-imaging methods. J. Magn. Reson. 54 (1983), 338.
72. MACFALL J. R., CHARLES H. C., BLACK R. D., et al.: Human lung air spaces: potential for MR imaging with hyperpolarized He-3. Radiology 200 (1996), 553.
73. MAKI J. H., CHENEVERT T. L. & PRINCE M. R.: Three-dimensional contrast-enhanced MR angiography. Top Magn. Reson. Imaging 8 (1996a), 322.
74. MAKI J. H., PRINCE M. R., LONDY F. J. & CHENEVERT T. L.: The effects of time varying intravascular signal intensity and *k*-space acquisition order on three-dimensional MR angiography image quality. J. Magn. Reson. Imaging 6 (1996b), 642.
75. MAKI J. H., WILSON G. J., EUBANK W. B. & HOOGEVEEN R. M.: Utilizing SENSE to achieve lower station sub-millimeter isotropic resolution and minimal venous enhancement in peripheral MR angiography. J. Magn. Reson. Imaging 15 (2002), 484.
76. MARCHAL G., BOSMANS H., VAN FRAEYENHOVEN L., et al.: Intracranial vascular lesions. optimization and

clinical evaluation of three-dimensional time-of-flight MR angiography. Radiology 175 (1990), 443.
77. MARCHAL G., BOSMANS H., VAN HECKE P., JIANG Y. B., AERTS P. & BAUER H.: Experimental Gd-DTPA polylysine enhanced MR angiography: sequence optimization. J. Comput. Assist. Tomogr. 15 (1991), 711.
78. MARTIN C. C., WILLIAMS R. F., GAO J. H., NICKERSON L. D., XIONG J. & FOX P. T.: The pharmacokinetics of hyperpolarized xenon: implications for cerebral MRI. J. Magn. Reson. Imaging 7 (1997), 848.
79. MASARYK T. J., MODIC M. T., ROSS J. S., et al.: Intracranial circulation: preliminary clinical results with three-dimensional (volume) MR angiography. Radiology 171 (1989a), 793.
80. MASARYK T. J., MODIC M. T., RUGGIERI P. M., et al.: Three-dimensional (volume) gradient-echo imaging of the carotid bifurcation: preliminary clinical experience. Radiology 171 (1989b), 801.
81. MASARYK T. J., ROSS J. S., MODIC M. T., LENZ G. W. & HAACKE E. M.: Carotid bifurcation. MR imaging. Work in progress. Radiology 166 (1988), 461.
82. MAZAHERI Y., CARROLL T. J. & DU J. , et al.: Combined time-resolved and high-spatial-resolution 3D MRA using an extended adaptive acquisition. J. Magn. Reson. Imaging 15 (2002), 291.
83. MAZAHERI Y., CARROLL T. J., KOROSEC F. R., et al.: High Resolution CE-MRA Using Dual-Resolution Acquisition and Segmentation Based on Spatial Frequency-Dependent 2D Temporal Correlation. Proceedings of the International Society for Magnetic Resonance in Medicine, 8th Scientific Meeting. Denver, USA 2000, p. 189.
84. MEANEY J. F., JOHANSSON L. O., AHLSTROM H. & PRINCE M. R.: Pulmonary magnetic resonance angiography. J. Magn. Reson. Imaging 10 (1999), 326.
85. MORAN P. R.: A flow velocity zeugmatographic interlace for NMR imaging in humans. Magn. Reson. Imaging 1 (1982), 197.
86. MUGLER J. P., DRIEHUYS B., BROOKEMAN J. R., et al.: MR imaging and spectroscopy using hyperpolarized ^{129}Xe gas: preliminary human results. Magn. Reson. Med. 37 (1997), 809.
87. MÖLLER H. E., CHAWLA M. S., CHEN X. J., et al.: Magnetic resonance angiography with hyperpolarized ^{129}Xe dissolved in a lipid emulsion. Magn. Reson. Med. 41 (1999), 1058.
88. MÖLLER H. E., CHEN X. J., SAAM B., et al.: of the lungs using hyperpolarized noble gases. Magn. Reson. Med. 47 (2002), 1029.
89. NAGELE T., KLOSE U., GRODD W., NUSSLIN F. & VOIGT K.: Nonlinear excitation profiles for three-dimensional inflow MR angiography. J. Magn. Reson. Imaging 5 (1995), 416.
90. OPPELT A., GRAUMANN R., BARFUSS H., FISCHER H., HARTL W. & SCHAJOR W.: FISP – a new fast MRI sequence. Electromedica 54 (1986), 15.
91. PARKER D. L., YUAN C. & BLATTER D. D.: MR angiography by multiple thin slab 3D acquisition. Magn. Reson. Med. 17 (1991), 434.
92. PELC N. J., BERNSTEIN M. A., SHIMAKAWA A. & GLOVER G. H.: Encoding strategies for three-direction phase-contrast MR imaging of flow. J. Magn. Reson. Imaging 1 (1991), 405.
93. PELED S., JOLESZ F. A., TSENG C. H., NASCIMBEN L., ALBERT M. S. & WALSWORTH R. L.: Determinants of tissue delivery for ^{129}Xe magnetic resonance in humans. Magn. Reson. Med. 36 (1996), 340.
94. PETERSSON D. C., KOROSEC F. R., GRIST T. M., et al.: Undersampled projection reconstruction applied to MR angiography. Magn. Reson. Med. 43 (2000), 91.
95. PETERSSON J. S.: k-Space models in MRI Using the Concept of Partitions. PhD Thesis. Lund University, Malmö 1998.
96. PETERSSON J. S. & CHRISTOFFERSSON J. O.: A multi-dimensional partition analysis of SSFP image pulse sequences. Magn. Reson. Imaging 15 (1997), 451.
97. PETERSSON J. S., CHRISTOFFERSSON J. O. & GOLMAN K.: MRI simulation using the *k*-space formalism. Magn. Reson. Imaging 11 (1993), 557.
98. PRIATNA A. & PASCHAL C. B.: Variable-angle uniform signal excitation (VUSE) for three-dimensional time-of-flight MR angiography. J. Magn. Reson. Imaging 5 (1995), 421.
99. PRINCE M. R. & GADOLINIUM-ENHANCED M. R.: aortography. Radiology 191 (1994), 155.
100. PRINCE M. R., CHENEVERT T. L., FOO T. K., LONDY F. J., WARD J. S. & MAKI J. H.: Contrast-enhanced abdominal MR angiography: optimization of imaging delay time by automating the detection of contrast material arrival in the aorta. Radiology 203 (1997), 109.
101. PRINCE M. R., NARASIMHAM D. L., STANLEY J. C., et al.: Breath-hold gadolinium-enhanced MR angiography of the abdominal aorta and its major branches. Radiology 197 (1995), 785.
102. PRINCE M. R., YUCEL E. K., KAUFMAN J. A., HARRISON D. C. & GELLER S. C.: Dynamic gadolinium-enhanced three-dimensional abdominal MR arteriography. J. Magn. Reson. Imaging 3 (1993), 877.
103. PRUESSMANN K. P., WEIGER M., SCHEIDEGGER M. B. & BOESIGER P.: SENSE. sensitivity encoding for fast MRI. Magn. Reson. Med. 42 (1999), 952.
104. PURDY D., CADENA G. & LAUB G.: The design of variable Tip-angle Slab Selection (TONE) pulses for improved 3D MR angiography. Proceedings of the Society of Magnetic Resonance Imaging. New York 1992, p. 882.
105. ROGOWSKA J.: Overview and Fundamentals of Medical Image Segmentation. In: Handbook of Medical Imaging, Processing and Analysis.Edited by I. N. BANKMAN. Academic Press, London 2000, p. 69.
106. RUGGIERI P. M., LAUB G. A., MASARYK T. J. & MODIC M. T.: Intracranial circulation: pulse-sequence considerations in three-dimensional (volume) MR angiography. Radiology 171 (1989), 785.
107. RUNGE V. M. & NELSON K. L.: Contrast Agents. In: Magnetic Resonance Imaging, Vol. 1. Edited by D. D. STARK & W. G. BRADLEY. Mosby Inc, St. Louis, Missouri, USA 1999, p. 257.
108. SAEED M., WENDLAND M. F. & HIGGINS C. B.: Blood pool MR contrast agents for cardiovascular imaging. J. Magn. Reson. Imaging 12 (2000), 890.
109. SALERNO M., ALTES T. A., MUGLER J. P., NAKATSU M., HATABU H. & DE LANGE E. E.: Hyperpolarized noble gas MR imaging of the lung: potential clinical applications. Eur. J. Radiol. 40 (2001), 33.
110. SALERNO M., DE LANGE E. E., ALTES T. A., TRUWIT J. D., BROOKEMAN J. R. & MUGLER J. P.: Emphysema. hyperpolarized helium 3 diffusion MR imaging of the lungs compared with spirometric indexes – initial experience. Radiology 222 (2002), 252.

111. SCHOENBERG S. O., BOCK M., FLOEMER F., et al.: High-resolution pulmonary arterio- and venography using multiple-bolus multiphase 3D-Gd-mRA. J. Magn. Reson. Imaging 10 (1999), 339.
112. SHETTY A. N., BIS K. G., KIRSCH M., WEINTRAUB J. & LAUB G.: Contrast-enhanced breath-hold three-dimensional magnetic resonance angiography in the evaluation of renal arteries: optimization of technique and pitfalls. J. Magn. Reson. Imaging 12 (2000), 912.
113. SHETTY A. N., BIS K. G., VRACHTOLIS T. G., KIRSCH M., SHIRKHODA A. & ELLWOOD R.: Contrast-enhanced 3D MRA with centric ordering in k space. A preliminary clinical experience in imaging the abdominal aorta and renal and peripheral arterial vasculature. J. Magn. Reson. Imaging 8 (1998), 603.
114. SODICKSON D. K. & MANNING W. J.: Simultaneous acquisition of spatial harmonics (SMASH): fast imaging with radiofrequency coil arrays. Magn. Reson. Med. 38 (1997), 591.
115. SODICKSON D. K., MCKENZIE C. A., LI W., WOLFF S., MANNING W. J. & EDELMAN R. R.: Contrast-enhanced 3D MR angiography with simultaneous acquisition of spatial harmonics: a pilot study. Radiology 217 (2000), 284.
116. STEFANCIK R. M. & SONKA M.: Highly automated segmentation of arterial and venous trees from three-dimensional magnetic resonance angiography (MRA). Int. J. Cardiovasc. Imaging 17 (2001), 37.
117. STEFFENS J. C., LINK J., GRASSNER J., et al.: Contrast-enhanced, K-space-centered, breath-hold MR angiography of the renal arteries and the abdominal aorta. J. Magn. Reson. Imaging 7 (1997), 617.
118. STROUSE P. J., PRINCE M. R. & CHENEVERT T. L.: Effect of the rate of gadopentetate dimeglumine administration on abdominal vascular and soft-tissue MR imaging enhancement patterns. Radiology 201 (1996), 809.
119. SUNDGREN P. C., SUNDEN P., LINDGREN A., LANKE J., HOLTAS S. & LARSSON E. M.: Carotid artery stenosis: contrast-enhanced MR angiography with two different scan times compared with digital subtraction angiography. Neuroradiology 44 (2002), 592.
120. SVENSSON J., MÅNSSON S., PETERSSON J. S. & OLSSON L. E.: Hyperpolarized ^{13}C MR angiography using trueFISP. Proc. International Society for Magnetic Resonance in Medicine, 10th Scientific Meeting. Honolulu, USA 2002, p. 2010.
121. SWANSON S. D., ROSEN M. S., AGRANOFF B. W., COULTER K. P., WELSH R. C. & CHUPP T. E.: Brain MRI with laser-polarized ^{129}Xe. Magn. Reson. Med. 38 (1997), 695.
122. TIZON X. & SMEDBY O.: Segmentation with gray-scale connectedness can separate arteries and veins in MRA. J. Magn. Reson. Imaging 15 (2002), 438.
123. TWIEG D. B.: The k-trajectory formulation of the NMR imaging process with applications in analysis and synthesis of imaging methods. Med. Phys. 10 (1983), 610.
124. VAN DER MEULEN P., GROEN J. P., TINUS A. M. & BRUNTINK G.: Fast Field Echo imaging. an overview and contrast calculations. Magn. Reson. Imaging 6 (1988), 355.
125. VIGEN K. K., PETERS D. C., GRIST T. M., BLOCK W. F. & MISTRETTA C. A.: Undersampled projection-reconstruction imaging for time-resolved contrast-enhanced imaging. Magn. Reson. Med. 43 (2000), 170.
126. VOSSHENRICH R. & FISCHER U.: Contrast-enhanced MR angiography of abdominal vessels: is there still a role for angiography? Eur. Radiol. 12 (2002), 218.
127. VRACHLIOTIS T. G., BIS K. G., SHETTY A. N. & RAVIKRISHAN K. P.: Contrast-enhanced three-dimensional MR angiography of the pulmonary vascular tree. Int. J. Cardiovasc. Imaging 18 (2002), 283.
128. WAGSHUL M. E., BUTTON T. M., LI H. F., et al.: *In vivo* MR imaging and spectroscopy using hyperpolarized ^{129}Xe. Magn. Reson. Med. 36 (1996), 183.
129. WALKER T. G. & HAPPER W.: Spin-exchange optical pumping of noble-gas nuclei. Rev. Mod. Phys. 69 (1997), 629.
130. WANG Y., JOHNSTON D. L., BREEN J. F. & HUSTON J., et al.: Dynamic MR digital subtraction angiography using contrast enhancement, fast data acquisition, and complex subtraction. Magn. Reson. Med. 36 (1996), 551.
131. WANG Y. YU Y., LI D., et al.: Artery and vein separation using susceptibility-dependent phase in contrast-enhanced MRA. J. Magn. Reson. Imaging 12 (2000), 661.
132. WEIGER M., PRUESSMANN K. P., KASSNER A., et al.: Contrast-enhanced 3D MRA using SENSE. J. Magn. Reson. Imaging 12 (2000), 671.
133. WEINMANN H. J., BRASCH R. C., PRESS W. R. & WESBEY G. E.: Characteristics of gadolinium-DTPA complex: a potential NMR contrast agent. Am. J. Roentgenol. 142 (1984), 619.
134. WILD J. M., SCHMIEDESKAMP J., PALEY M. N. J., et al.: MR imaging of the lungs with hyperpolarized helium-3 gas transported by air. Phys. Med. Biol. 47 (2002), N185.
135. WILMAN A. H. & RIEDERER S. J.: Performance of an elliptical centric view order for signal enhancement and motion artifact suppression in breath-hold three-dimensional gradient echo imaging. Magn. Reson. Med. 38 (1997a), 793.
136. WILMAN A. H., RIEDERER S. J., KING B. F., DEBBINS J. P., ROSSMAN P. J. & EHMAN R. L.: Fluoroscopically triggered contrast-enhanced three-dimensional MR angiography with elliptical centric view order: application to the renal arteries. Radiology 205 (1997b), 137.
137. WOLBER J., ROWLAND I. J., LEACH M. O. & BIFONE A.: Perfluorocarbon emulsions as intravenous delivery media for hyperpolarized xenon. Magn. Reson. Med. 41 (1999), 442.